New developments in high field electron paramagnetic resonance with applications in structural biology

2005 Rep. Prog. Phys. 68 411

(http://iopscience.iop.org/0034-4885/68/2/R05)

INSTITUTE OF PHYSICS PUBLISHING REPORTS ON PROGRESS IN PHYSICS

Rep. Prog. Phys. **68** (2005) 411–448 doi:10.1088/0034-4885/68/2/R05

New developments in high field electron paramagnetic resonance with applications in structural biology

Marina Bennati and Thomas F Prisner

Institute of Physical and Theoretical Chemistry and Center for Biomolecular Magnetic Resonance, Johann Wolfgang Goethe-University Frankfurt, Marie-Curie-Strasse 11, D-60439 Frankfurt, Germany

E-mail: prisner@chemie.uni-frankfurt.de and bennati@chemie.uni-frankfurt.de

Received 5 August 2004
Published 18 January 2005
Online at stacks.iop.org/RoPP/68/411

Abstract

Recent developments in microwave technologies have led to a renaissance of electron paramagnetic resonance (EPR) due to the implementation of new spectrometers operating at frequencies $\geqslant$90 GHz. EPR at high fields and high frequencies (HF-EPR) has been established up to THz (very high frequency (VHF) EPR) in continuous wave (cw) operation and up to about 300 GHz in pulsed operation. To date, its most prominent application field is structural biology. This review article first gives an overview of the theoretical basics and the technical aspects of HF-EPR methodologies, such as cw and pulsed HF-EPR, as well as electron nuclear double resonance at high fields (HF-ENDOR). In the second part, the article illustrates different application areas of HF-EPR in studies of protein structure and function. In particular, HF-EPR has delivered essential contributions to disentangling complex spectra of radical cofactors or reaction intermediates in photosynthetic reaction centres, radical enzymes (such as ribonucleotide reductase) and in metalloproteins. Furthermore, HF-EPR combined with site-directed spin labelling in membranes and soluble proteins provides new methods of investigating complex molecular dynamics and intermolecular distances.

(Some figures in this article are in colour only in the electronic version)

Contents

1. Introduction

Paramagnetic molecules play an important functional role in proteins and ribozymes, acting in many cases as active centres for electron transfer and catalytic reactions. Electron paramagnetic resonance (EPR) spectroscopy has become an essential tool for the investigation of such cofactors. The most widely employed EPR technique utilizes continuous wave (cw) irradiation at standard X-band frequencies (9 GHz) while performing a magnetic field sweep to obtain the spectra. However, the resulting spectra can be very complex and the spectral resolution quite poor, in particular when more than one paramagnetic species is present, as is often the case in biological samples. There have been three important methodological developments to overcome this problem: (1) the use of higher microwave frequencies and, respectively, higher magnetic fields in high field EPR (HF-EPR) to spread the spectra in the field dimension; (2) pulsed EPR methods, which add a new dimension (a time axis) to the spectra and (3) double resonance techniques, such as ENDOR (Electron Nuclear DOuble Resonance) or ELDOR (Electron–Electron DOuble Resonance), which allow excitation of two spins (either an electron spin and a nuclear spin or two electron spins) to specifically measure the spin–spin coupling.

HF-EPR denotes EPR spectroscopy performed at microwave (MW) frequencies of about 90 GHz or higher, corresponding to a magnetic field of $B_0 > 3$ T. Its intrinsic advantage consists in the ability to resolve g-values when g-anisotropy ($\Delta g/g_{\mathrm{iso}}$) is typically much less than 1%. Pulsed EPR methods as well as double resonance methods can both be combined with HF-EPR but the technical realization is much more demanding than at X-band frequencies.

Two classes of paramagnetic molecules are naturally encountered in biological systems: aromatic organic radicals, such as quinones, amino or nucleic acids, which can form transient paramagnetic states in electron transfer reactions, and transition metal ions or complexes, such as haemes or FeS clusters, which mediate and catalyze reactions by their different oxidation states. For both classes, the extension of EPR spectroscopy to high magnetic field strengths and accordingly high microwave frequencies has substantially increased the potential to characterize the structural and functional properties of the cofactors involved. First applications of HF-EPR on biological systems go back to 1973, when Alpert and co-workers analysed the high-spin ferric Fe^{3+} ion ($S = \frac{5}{2}$) of acid methemoglobin with frequencies up to 372 GHz and magnetic field strengths up to 6 T (Alpert *et al* 1973). Since then, structural biology has become the most prominent application field of this new method.

This review article will start with a short description of the parameters that can be determined by EPR spectroscopy (section 2), having a focus on those relevant for HF-EPR on biological applications. The following sections will give an overview of the current state of the art in instrumentation (section 3) and an introduction to the methodology of HF-EPR, such as cw HF-EPR (section 4), pulsed HF-EPR (section 5) and electron nuclear double resonance (HF-ENDOR) (section 6). These sections focus on the latest developments, because numerous very good reviews about the general method and specific technical aspects of HF-EPR already exist (see, e.g. Grinberg and Berliner (2004) and references therein). In section 7, we will report new applications of these techniques on biological systems. This section is structured with respect to the major classes of paramagnetic molecules: organic radicals, transition metal ions and nitroxide spin labels. It begins with photosynthetic proteins and ribonucleotide reductase, the two classes of protein complexes that have been prototypes for understanding the role of organic cofactors. Other examples of aromatic organic radicals in proteins follow. Within the class of transition metal ions, manganese and copper proteins are the most extensively studied by HF-EPR and ENDOR. Finally, the last section gives a short overview of the increasingly popular field of HF-EPR on nitroxide spin labels in membranes, proteins and oligonucleotides.

2. Theory

The interaction of the unpaired electron spin of a paramagnetic molecule with the external and internal magnetic fields can be described by the electron spin Hamiltonian

$$H = H_0 + H_{\mathrm{mw}}(t), \tag{1}$$

where $H_{\mathrm{mw}}(t)$ is the interaction of the magnetic moment of the unpaired electron spin with the oscillating external microwave field and H_0 is the static spin Hamiltonian given by

$$H_0 = H_{\mathrm{Z}} \sum_S (H_{\mathrm{D}}^S + H_{\mathrm{J}}^S) + \sum_I (H_{\mathrm{Z}}^I + H_{\mathrm{A}}^I + H_{\mathrm{Q}}^I). \tag{2}$$

H_{Z} is the electron Zeeman Hamiltonian and describes the interaction of the unpaired electron spin with the static external magnetic field B_0:

$$H_{\mathrm{Z}} = h \cdot \beta_{\mathrm{e}} \cdot \hat{\vec{S}} \cdot \tilde{G} \cdot \vec{B}_0, \tag{3}$$

where h is the Planck constant, β_{e} the Bohr magneton, $\hat{\vec{S}} = (\hat{S}_x, \hat{S}_y, \hat{S}_z)$ the Pauli spin operator vector and $\tilde{G}$ is the 3×3 G-matrix. This interaction leads to energy eigenvalues that scale with the external magnetic field. At high magnetic field values, the microwave resonance frequency (Larmor frequency) is given by the relation

$$\upsilon_{\mathrm{L}} = \beta_{\mathrm{e}} \cdot g_{\mathrm{eff}}(\theta, \varphi) \cdot B_0 \tag{4}$$

with

$$g_{\mathrm{eff}}(\theta, \varphi) = \sqrt{\sin^2\theta \cdot \cos^2\varphi \cdot g_x^2 + \sin^2\theta \cdot \sin^2\varphi \cdot g_y^2 + \cos^2\theta \cdot g_z^2}, \tag{5}$$

where θ and φ are the polar angles of the magnetic field direction within the molecular G-tensor axis system. Therefore, the population difference of these states given by the Boltzmann law is larger at higher magnetic field values. Nevertheless, the absolute spin polarization at a microwave resonance frequency of 100 GHz is still very small (1.6% at room temperature). The temperature that corresponds to the Zeeman splitting is about 4.8 K; therefore, at liquid helium temperatures the upper level is already depleted, which implies effects on the relaxation rates and allows the determination of the sign of dipolar and hyperfine coupling constants.

Because most other interactions are not field dependent, the Zeeman interaction will become dominant at large values of the magnetic field and HF-EPR permits us to resolve the main G-matrix elements (g_x, g_y, g_z) of the paramagnetic centre. The deviation of the main g-values from the free electron g_{e}-value (2.0023) arises from residual orbital momentum of the unpaired electron. These values can be used as a simple fingerprint to identify the radical species or in comparison with quantum chemical calculations to investigate the hydrogen or ligand binding geometry and the electrostatic surrounding of the paramagnetic molecule in the protein.

If the G-tensor is not isotropic, molecules with different orientations with respect to the external magnetic field will have distinct resonance field values. In disordered samples, as typical for biological systems, this allows the selection experimentally of only those molecules with a specific orientation with respect to the external magnetic field. This so-called orientation selection enables us to extract the anisotropy of other interactions and their main axis orientation within the given G-tensor axis system. The method is particularly helpful for the measurement of anisotropic interactions to other close-by nuclear or electronic spins, such as hyperfine and dipolar couplings, to obtain structural data.

To resolve the main G-matrix elements, the difference in the Larmor resonance frequencies has to be larger than other linewidth contributions, such as unresolved hyperfine interactions, which do not scale with the external magnetic field. Typical linewidths of organic radicals

with unresolved hyperfine couplings are about 10–30 MHz. For such radicals, the anisotropy of the G-matrix, defined as

$$\Delta g = \max(\tilde{G}) - \min(\tilde{G}) \tag{6}$$

is typically of the order of 10^{-3}–10^{-4}. Therefore microwave frequencies of more than 70 GHz are required to resolve the G-tensor anisotropy. This can be used for a definition of *high frequency EPR*:

$$\frac{\Delta g}{g_{\mathrm{iso}}} B_0 > \Delta B_{1/2}^{\mathrm{hfi}} \tag{7}$$

and the isotropic g-value is given by

$$g_{\mathrm{iso}} = \tfrac{1}{3}\mathrm{trace}(\tilde{G}). \tag{8}$$

We note that this definition of HF-EPR is related to the sample properties and it is not of universal use. As will be shown later on, for some organic radicals, microwave frequencies larger than 300 GHz are necessary to fulfil this condition. The increased resolution can only be achieved if the broadening mechanisms are not (or less) field dependent. This would not be the case if the resolution were limited by a distribution of g-values (G-strain), introduced by intrinsic inhomogeneities of the paramagnetic molecules in the macroscopic sample. Fortunately, this is typically not the case for paramagnetic centres in biological samples.

If more than one paramagnetic species is present in the protein, H_{D}^{S} describes the magnetic dipole–dipole interaction and H_{J}^{S} the Heisenberg exchange interaction between the two spins. The respective Hamiltonians between two electron spins S_1 and S_2 can be written as:

$$H_{\mathrm{D}} = h \cdot \hat{\tilde{S}}_1 \cdot \tilde{D} \cdot \hat{\tilde{S}}_2, \qquad H_{\mathrm{J}} = h \cdot J \cdot \hat{\tilde{S}}_1 \cdot \hat{\tilde{S}}_2. \tag{9}$$

In this notation $\tilde{D}$ is a traceless axial 2nd rank tensor, which can be fully described by the scalar dipolar coupling constant $D_{||}$, and J is the isotropic exchange coupling constant. In the high field approximation ($D_{||} \ll B_0$) the dipolar Hamiltonian can be written as

$$H_{\mathrm{D}} = \frac{\mu_0}{4\pi} \frac{g_1^{\mathrm{eff}} \cdot g_2^{\mathrm{eff}}}{r^3} \cdot (3 \cdot \cos^2(\theta) - 1) \cdot \hat{S}_z^1 \cdot \hat{S}_z^2, \tag{10}$$

where r is the distance between spins 1 and 2 and θ is the angle between the interconnecting vector and the external magnetic field direction. Therefore, the determination of this interaction allows the measurement of the distance r between two close-by spins. In cw-EPR experiments, this is usually only possible for distances $r < 2$ nm, because of other spectral broadening contributions. In pulsed experiments some of the other interactions can be eliminated and distances up to $r = 8$ nm can be detected. If, as explained before, specific oriented molecules are selected by their anisotropic g-values, the orientation of the interconnecting vector between the two paramagnetic centres, with respect to the G-matrix axis system of the observer spin, can be additionally determined. The exchange interaction decays exponentially with the distance r and can usually only be detected for distances $r < 1$ nm.

For high spin systems ($S > \frac{1}{2}$), as for transition metal ions, the same notation with $S_1 = S_2 = S$ can be used to calculate the zero-field splitting (ZFS) and the exchange interaction. These interactions can be very strong, even in biological metal centres. In such cases, high magnetic fields are necessary to simplify the spectra (high field approximation) or even to achieve a resonance condition (section 4).

The last three terms of equation (2) describe the interaction of nuclei (with a nuclear spin I) in the close surrounding of the paramagnetic molecule ($r < 0.8$ nm) with the unpaired electron spin or with the external fields. The first term H_{Z}^{I} describes the Zeeman splitting of the nuclear spin. Because of the much smaller gyromagnetic ratio, these splittings are 3–4 orders of magnitude smaller than the electron Zeeman splitting. The second term describes the interaction of the magnetic moment of the nuclear spin with the magnetic moment of the

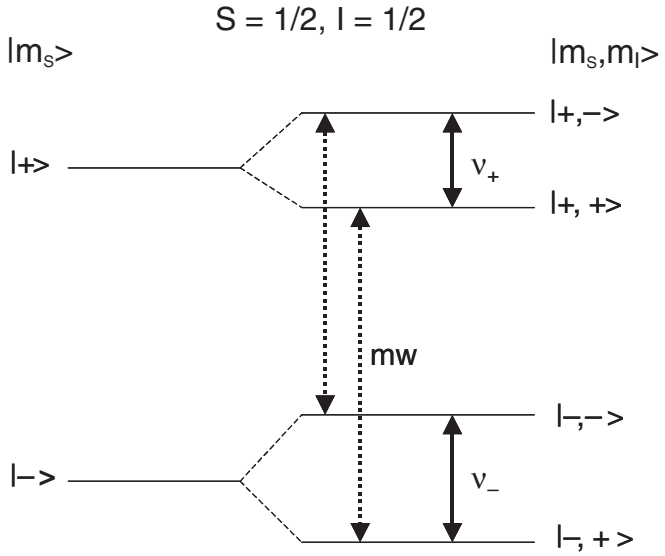

Figure 1. Schematic energy level diagram for an electron spin $S = \frac{1}{2}$ coupled to one nucleus $I = \frac{1}{2}$ with a positive hyperfine coupling A smaller than the nuclear Zeeman frequency. The dotted lines represent EPR (mw) transitions and the solid lines are nuclear (or ENDOR) transitions. The symbols $\pm$ are abbreviations for the electron and nuclear Zeeman eigenstates $m_S = \pm\frac{1}{2}$ and $m_I = \pm\frac{1}{2}$.

electron spin. As for the interaction between two electron spins, it can be decomposed into two parts: an anisotropic hyperfine tensor $\tilde{A}_{\text{aniso}}$, which describes the through-space dipole–dipole interactions and an isotropic coupling a_{iso}, which arises from electron spin density at the nucleus (Fermi contact interaction) and polarization effects of the inner shell electrons.

$$H_{\text{A}} = h \cdot \hat{\vec{S}} \cdot \tilde{A} \cdot \hat{\vec{I}} = h \cdot (\hat{\vec{S}} \cdot \tilde{A}_{\text{aniso}} \cdot \hat{\vec{I}} + a_{\text{iso}} \cdot \hat{\vec{S}} \cdot \hat{\vec{I}}). \tag{11}$$

A simple energy diagram consisting of one electron spin, $S = \frac{1}{2}$, coupled to a single nuclear spin, $I = \frac{1}{2}$ (such as a proton) is schematically shown in figure 1.

The last term describes the quadrupole interaction for nuclei with a nuclear spin $I \geqslant 1$:

$$H_{\text{Q}} = h \cdot \hat{\vec{I}} \cdot \tilde{Q} \cdot \hat{\vec{I}}. \tag{12}$$

Whereas the hyperfine and quadrupole interactions are not field dependent, the nuclear Zeeman interaction again scales linearly with the external field. This leads to a simplification of the spectra, if the nuclear Zeeman interaction exceeds the hyperfine coupling. In this case, the nuclear spin also becomes quantized in the direction of the external magnetic field (high field approximation for the nuclear spin) and forbidden EPR transitions ($\Delta m_I = \pm 1$) are suppressed. Additionally, this allows a much better separation of the nuclear resonances by ENDOR, as will be explained in more detail later on.

All the interactions discussed above can also become time dependent, either by motion or spin dynamics, leading to changes in the line shape of the spectra and to relaxation processes. The EPR experiment is sensitive to fluctuations in the ns time range and at the inverse of the Larmor frequency (in radians). Therefore, the relaxation behaviour also has a frequency (and field) dependence. Additional field dependence of the relaxation rate may occur if the fluctuating interaction is itself field dependent, as for example the electron Zeeman interaction. The anisotropy of the G-matrix will lead to a modulation of the Larmor frequency for rotating

molecules. Usually, in proteins, the rotational motion is too slow to contribute to the relaxation process, but librational small angle motions of the paramagnetic molecule may be observable at high magnetic field strengths.

3. Instrumentation

The first high resolution cw HF-EPR spectrometer was developed in Moscow by Lebedev at a MW frequency of 140 GHz (Ondar *et al* 1983). Further on, the first HF pulsed EPR spectrometer was built in Leiden at 95 GHz (Weber *et al* 1989). Since 1996, a 95 GHz pulsed HF-EPR spectrometer has been offered commercially by Bruker Analytik (Höfer *et al* 1996), as well as by Donetsk Physico Technical Institute (Goldfarb and Krymov 2004) at 95 and 140 GHz microwave frequencies. Numerous recent review articles exist, which discuss the main technical issues of cw and pulsed HF-EPR spectrometers (Prisner 1997, 2004, Freed 2000, Smith and Riedi 2000). In this chapter we will therefore restrict the discussion to the current state of the art of the instrumentation.

The implementation of HF-EPR spectrometers has been greatly facilitated by substantial progress in microwave as well as in high magnetic field technologies that has occurred over the past two decades. Today, superconducting magnets are commercially available up to 22 T, permitting construction of EPR spectrometers up to 600 GHz. For cw HF-EPR, low power microwave sources or lasers can be used for excitation and no cavity resonance structure is needed; thus, the magnetic field has become the limiting factor for a further increase of frequencies (Muller *et al* 1989, Brunel *et al* 1995). Spectrometers with cw-FIR lasers as submillimetre wave sources have been developed up to THz at national large scale facilities for high magnetic fields (Schneider-Muntau *et al* 2004).

In contrast, pulsed HF-EPR spectrometers have only become widespread at frequencies up to 140 GHz. Only two home-built spectrometers that permit routine spectroscopy have been reported so far at higher microwave frequencies, the first one at 180 GHz (Rohrer *et al* 2001a) with recently implemented pulsed ENDOR and ELDOR capabilities, the second at 270 GHz (Blok *et al* 2004b) with pulsed ENDOR capabilities. The possible extension to even higher frequencies has been demonstrated at 604 GHz using pulsed far infrared lasers, a Fabry–Perot cavity and Schottky diodes as mixer elements (Kutter *et al* 1995). To illustrate one of the new technical developments of pulsed HF-EPR, we display in figure 2 our first two-frequency three-pulse electron–electron double resonance (PELDOR) experiment recorded at 180 GHz. The echo modulation reflects the 33 Å distance between two tyrosyl radicals in the enzyme RNR from *E. coli*. For this type of experiments (Milov *et al* 1984) a second microwave frequency has to be implemented for the excitation. The experiments were realized by combining a second microwave source and some modifications in the high-power arm of our home-built 180 GHz microwave bridge to achieve a sufficient power level for pump and detection pulses (Denisenkov *et al* 2004). Similar extensions of pulsed HF-EPR spectrometers are under construction in other laboratories and on the commercial HF-EPR system from Bruker (Carl *et al* 2004).

Different reasons can be attributed to the current limits in frequency for pulsed HF-EPR. First, classical spectrometer designs with a microwave resonator operating in reflection mode and commercial MW components such as wave guides and MW circulators are feasible only up to about 150 GHz. At higher frequencies, the small wavelengths cause dramatic power losses in rectangular wave guides and quasi-optical components have to be introduced (Lynch *et al* 1988, Smith *et al* 1998, Cardin *et al* 1999, Fuchs *et al* 1999, Hassan *et al* 1999, Rohrer *et al* 2001a, Blok *et al* 2004b). Furthermore, pulsed EPR intrinsically requires a substantial microwave B_1-field strength at the sample position to obtain pulses of reasonable lengths compared to

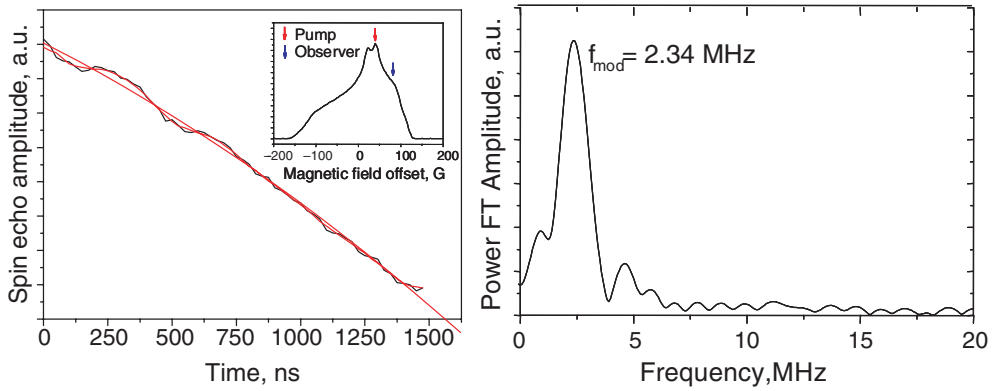

Figure 2. Left: 180 GHz three-pulse DEER modulation trace of approx. 1 mM R2 protein from *E. coli* RNR. The inset displays the echo-detected EPR spectrum of the tyrosyl radical pair with the position of the pumping and detection frequency. Right: the Fourier transformation was obtained after fitting and subtracting the intrinsic echo-decay function. Due to orientational selectivity, the observed modulation frequency does not correspond to any of the canonical values ($D_{||} = 2 * D_{\perp}$) of the dipolar tensor, which are best determined from X-band data (Bennati *et al* 2003). The two-dimensional experiment at high field, where the dipolar frequency is determined as a function of the pumping and detecting frequency, allows the unique determination of the mutual orientation of the two radicals.

the electron spin relaxation times ($B_1 \approx 1$ G for $t_{\pi/2} < 100$ ns). This is usually achieved by combining medium microwave power (10–100 mW) with a high quality resonance structure. However, conventional solid-state microwave sources display an output power that scales with $1/\nu^2$ (Bhartia and Bahl 1984), with typically 10–20 mW in the range of 100–200 GHz. Concomitantly, the dimensions of fundamental cavities scale with $1/\nu$, conferring crucial limits on the already miniature samples used. The 270 GHz pulsed EPR spectrometer developed by Blok *et al* (2004b) might have reached the limit of this technology.

High power (>100 mW) sources, such as gyrotrons (Becerra *et al* 1993, Bajaj *et al* 2003), EIOs (Prisner *et al* 1992) or orotrons (Grishin *et al* 2004) have been proposed for HF-pulsed EPR to circumvent the described limitations and would be compatible with oversized low-Q cavities or with Fabry–Perot resonators. However, external switching of these sources with pin diodes is technically not feasible whereas internal switching often causes incoherences between pulses. Much more advantageous would be the availability of microwave amplifiers (such as gyroamplifiers, or EIAs), since it would permit us to control pulse switching at lower power and lower frequencies using upconversion schemes. The prototype of such a spectrometer at 95 GHz, based on a 1 kW EIK amplifier, has been recently presented by Freed and co-workers (Hofbauer *et al* 2004). The spectrometer achieves $\pi/2$-pulse lengths as short as 4 ns and an estimated bandwidth of about 200 MHz. This allows full irradiation of EPR lines of typical organic radicals and offers the possibility for sophisticated two-dimensional-correlation experiments with phase cycling at high frequencies.

4. CW EPR at high fields

4.1. Technical aspects

For biological samples with low concentrations of paramagnetic molecules, the sensitivity of the EPR set-up is of utmost importance. Typical concentrations of membrane bound

metalloenzymes of 100 μM in a sample volume of 10 μl and with a spectral width of 0.1 T require a sensitivity of at least 10^{12} spins/(mT$\sqrt{\text{Hz}}$) for a routine detection. This is approximately the sensitivity that can be achieved with a transmission mode set-up without a microwave resonant structure, where the absorption of the microwave is directly measured (Muller *et al* 1989, Hassan *et al* 1999, Un *et al* 2001a). The absolute sensitivity of a reflection mode set-up with a resonant microwave cavity can be several orders of magnitudes higher (Prisner *et al* 1994), but at the same time the effective sample volume is reduced by 1–3 orders of magnitude, depending on the microwave frequency and resonant structure (typically below 1 μl at 200 GHz). This usually leads to a superior sensitivity for the EPR set-up with a resonant microwave structure, but the adjustment of the experiment is more demanding and the handling of the tiny sample more difficult. For trapping of transient paramagnetic states in enzymes the sample has to be kept cold (<100 K) after freeze quenching. This procedure is more challenging for the small sample capillaries used in cylindrical resonators. The other important limiting factor for cw-EPR sensitivity of broad spectral lines is the maximum available modulation field strength. Again, this can be achieved more easily in a transmission mode set-up, which is less sensitive to microphonic effects, compared to a reflection mode resonant cavity set-up. On the other hand, a transmission mode set-up without cavity cannot be extended to pulse or ENDOR operation. Therefore, both set-ups have their advantages and disadvantages for specific applications.

4.2. Spin $\frac{1}{2}$ systems

For biological applications, the class of $S = \frac{1}{2}$ systems mainly consists of aromatic organic cofactors, such as for example chlorophylls and quinones, amino or nucleotide acid radicals, such as tyrosine or guanine, and nitroxide spin labels. For such $S = \frac{1}{2}$ spin systems, the main advantage of cw HF-EPR applications is the resolution of the anisotropic G-tensor, which can only be achieved at high magnetic field values, as explained above. Examples of such experiments will be described in section 7.

In single crystal samples, cw HF-EPR can also be advantageous for other paramagnetic species, where usually the G-tensor is fully resolved at lower microwave frequencies, because the higher spectral resolution at high fields allows different sites in the crystal to be distinguished and gives a much better sensitivity for small samples (Coremans *et al* 1996). As an example, such a single crystal study on photosystem II of cyanobacterium *Synechococcus elongatus* is displayed in figure 3 (Hofbauer *et al* 2001).

Cw HF-EPR spectra at 94 GHz are shown as a function of the rotation angle of the crystal with respect to the magnetic field direction (for two different rotation planes). There are up to eight magnetically non-equivalent tyrosyl radicals Y_{D}, depending on the crystal orientation because there are four different PSII dimers in the unit cell. Their spectral centre position is shown by the lines drawn in rotation patterns. The spectra of each tyrosyl radical is further complicated by hyperfine coupling of the ring protons. Nevertheless, the spectral resolution at high magnetic fields was high enough to resolve all different sites and simulate the rotation pattern in impressive detail. From these data, the orientation of the tyrosyl radical Y_{D} in PSII could be determined.

4.3. High spin systems

The biologically important group of transition metal ions and complexes, such as Mn or Fe, belong to the second class of paramagnetic molecules, the high spin systems. These systems exhibit an additional interaction, the ZFS. In the simplest approximation this interaction

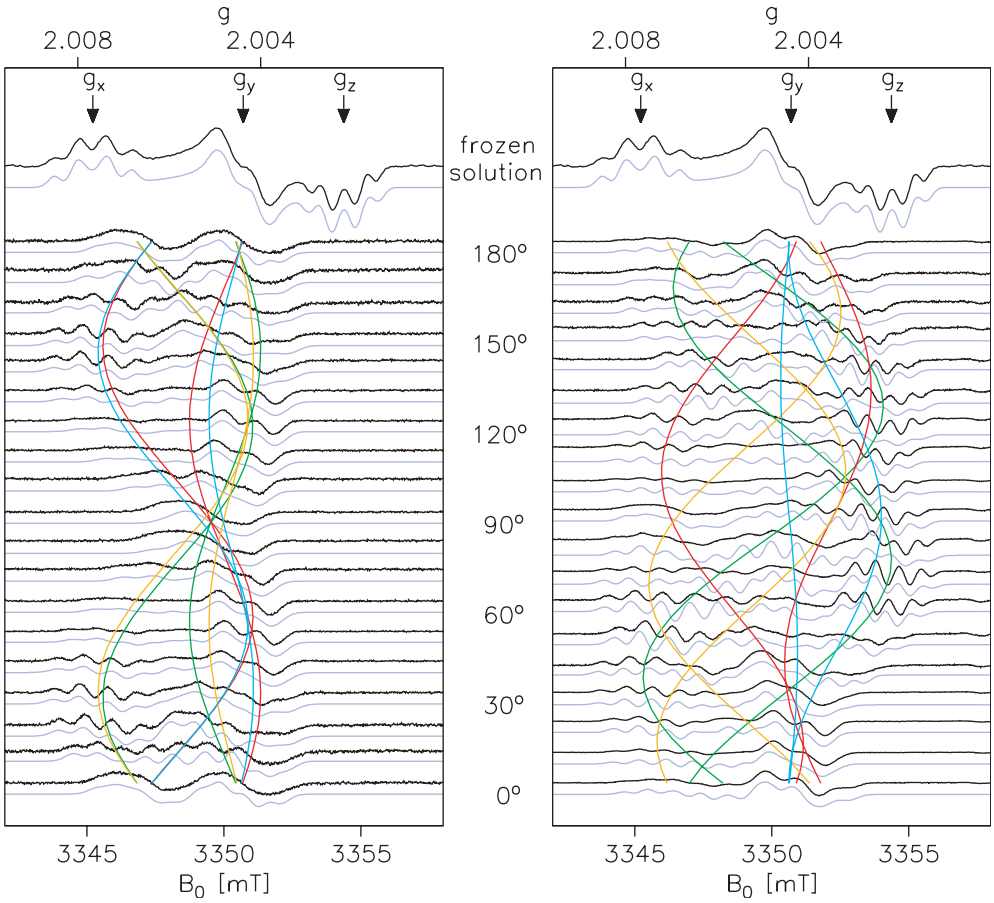

Figure 3. 94 GHz cw EPR spectra (black, experiment; light blue, simulation) of Y_D in frozen solution (top) and single crystals (rotation patterns) of PSII cc from *S. elongatus*, adapted with permission from (Hofbauer *et al* 2001). Left: crystal rotated approximately about the crystallographic *a* axis. Right: arbitrary rotation axis. Coloured lines indicate the calculated angular dependence of the effective g-value for each Y_D residue in the unit cell.

can be described by a traceless tensor of second rank and by the two scalar parameters D (ZFS constant) and E (asymmetry parameter). Two different experimental situations can be distinguished, depending on the ratio of the ZFS constant and the external magnetic field strength. If the ZFS is larger than the electron Zeeman splitting, the electron spin is quantized in the ZFS frame, which is related to the local structure of the metal ion in the protein. The microwave excitation and selection rules that apply to this basis system are different from the so-called high field case, where the Zeeman interaction is much larger than the zero-field interaction and where the electron spin is quantized along the magnetic field direction. The intermediate case, where both interactions are of similar strength, is particularly difficult to analyse quantitatively, because the two bases are not eigenstates of the spin system. The situation is often further complicated, because many important transition metal ions, such as for example Mn, Cu or Fe, exhibit an additional nuclear spin $I > \frac{1}{2}$ with a strong hyperfine coupling. Because for many biological metal ions the ZFS constant D is easily in the range of 1 T or above, high magnetic fields are necessary to obtain simple spectra.

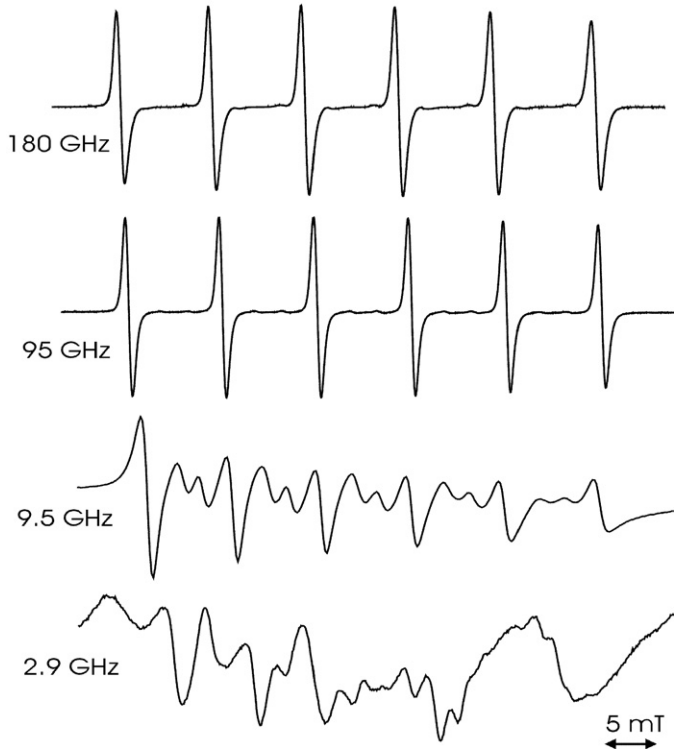

Figure 4. Multifrequency cw EPR spectra of the protein nucleotide complex p21ras·Mn^{2+}·GDP in frozen solution; reproduced with permission from Rohrer *et al* (2001a).

For half-integer high spin systems, such as for example high-spin Fe^{3+} or Mn^{2+} ions, a twofold degeneracy of the spin states remain (Kramer's doublet). The transitions between these Zeeman split pairs can be observed even at low magnetic field strengths. The central transition from $m_S = +\frac{1}{2}$ to $m_S = -\frac{1}{2}$ is only effected in second-order perturbation by the ZFS interaction and becomes substantially narrowed ($\propto B_0/D$) at higher magnetic field values. This leads to a very high sensitivity to such paramagnetic ions and allows an improved detection of superhyperfine coupling to the ligand sphere nuclei. The other transitions are broad and can, in general, only be observed if the microwave frequency is larger than the ZFS constant. An example of the magnetic field dependence of a Mn^{2+} ion spectrum in a complex with the protein p21ras and the nucleotide GDP is shown in figure 4.

A substantial narrowing of the central transition $m_S = +\frac{1}{2}$ to $m_S = -\frac{1}{2}$ can be observed by increasing the field from 0.1 to 6.4 T. The ZFS constant in this complex is only $D \approx 20$ mT. Therefore, already at 3.4 T the linewidth contribution from ZFS is rather small and other superhyperfine couplings to ligand nuclei can be observed with high sensitivity, as will be explained in more detail in section 7.

For integer high spin systems, all transitions depend, to first order, on the zero-field interaction. Therefore, such systems, for example Mn^{3+} or Mn-clusters, might show no EPR transition at all if the microwave frequency is too small and are called 'EPR-silent' (Hagen 1999). Their ZFS parameters and G-tensor values can only be extracted correctly if the experiments are performed at high microwave frequencies and with extremely broad magnetic field sweeps. In this case, the main coil of the superconducting magnet or the electromagnetic

Bitter magnet has to be swept differently than for organic aromatic radicals, where additional sweep coils are sufficient to cover the spectral width.

5. Pulsed EPR

5.1. Technical aspects

At lower microwave frequencies the sensitivity of the pulsed EPR experiments are reduced in comparison with cw-EPR experiments, because the bandwidth of the resonant circuit has to be increased (and therefore the quality factor Q of the cavity, defined as bandwidth divided by the microwave frequency, has to be lowered) to transmit short microwave pulses in the ns range. This is different at high microwave frequencies, because the typical Q values achievable for fundamental mode cavities lead to a sufficient bandwidth for the achievable microwave pulse lengths. Because pulsed EPR does not suffer from microphonic noise arising from the field modulation techniques applied in cw-EPR experiments, pulsed HF-EPR experiments offer better signal-to-noise performance and background stability than cw experiments.

As explained above, fundamental mode resonance structures are necessary to obtain reasonably short microwave pulses. The most important parameter is the conversion factor c, describing the efficiency of conversion of microwave power P_{mw} to magnetic field strength B_1 for a specific type of cavity:

$$B_1 = c \cdot \sqrt{Q \cdot P_{\mathrm{mw}}}. \tag{13}$$

The conversion factor c for a given type of cavity depends on the microwave frequency:

$$c \propto \sqrt{\frac{\mu_0}{V_c \cdot \nu_{\mathrm{mw}}}} \approx \sqrt{\mu_0} \cdot \nu_{\mathrm{mw}}. \tag{14}$$

As can be seen from this formula, the conversion factor improves by going to higher microwave frequencies. This allows the achievement of reasonably short pulse lengths with lower excitation powers. Fundamental cylindrical cavities (TE_{011}) have been widely used at high-frequencies (Prisner 1997, Rohrer *et al* 2001a, Blok *et al* 2004b) for pulsed measurements because of a conversion factor that is one order of magnitude better compared to Fabry–Perot resonators (Earle *et al* 1996, Smith *et al* 1998). Additionally, the high conversion and filling factor and the stronger magnetization at higher fields will give rise to large induced microwave signals. This leads to an increased absolute sensitivity of HF-EPR spectrometers compared to conventional X-band frequencies.

5.2. Transient paramagnetic states

Electron transfer reactions in proteins can be triggered by photoexcitation either naturally, such as for example in photosynthetic proteins, or artificially. After the laser flash, transient (cw) or pulsed EPR methods can be used to detect the transient paramagnetic species within the electron transfer reaction. The time resolution of the transient EPR detection method is limited by the bandwidth of the microwave detection system and of the microwave resonant cavity. For the pulsed detection, the limiting factor is the typical pulse length for an optimal excitation of the spin system. In both cases, this is currently of the order of 10–100 ns for existing set-ups, limiting the observation to rather slow reaction steps in the electron transfer reaction pathway. For such transient species, the pulsed EPR detection has a sensitivity as high as for stable radicals and is only limited by the repetition rate of the photocycle, which is different from cw-EPR detection (Prisner 2004). In contrast to transient EPR detection,

the pulsed method allows the detection of the reaction and spin kinetics without any possible distortion given by an extended time microwave irradiation.

Further improvements in the time resolution can be envisaged in the future by higher microwave excitation power and respectively shorter pulse lengths. At the same time, the bandwidth of the resonant microwave structure and of the detection channel has to be enlarged, which will lower the ringing time after the strong excitation pulses but also reduce the sensitivity. Consequently, decoupling of the detection channel from the strong excitation pulses is necessary to obtain a time resolution in the small ns or sub-ns range. This can be achieved by an induction mode detection of the signal, where the orthogonal signal component of the circularly polarized signal with respect to the linearly polarized excitation is detected. With Fabry–Perot resonators a decoupling of up to 6 orders of magnitude can be realized (Prisner *et al* 1992, Smith *et al* 1998).

5.3. Separation of radicals

Another advantage of pulsed EPR detection compared to the cw-EPR method is the possibility of separating overlapping spectral components of different paramagnetic species. These methods are based either on the different relaxation properties (T_1 or T_2) of the species involved or on their different transition moments (Schweiger and Jeschke 2001) (Hofbauer and Bittl 2000). At high fields, the combination of these methods with the additional G-resolution becomes a powerful tool for the assignment of the observed signals. An example of the capability of this method is shown in figure 5, where a three-pulse stimulated echo sequence at 140 GHz was used to separate the spectrally overlapping signals of three radicals, a tyrosyl radical, an organic carbon-centred radical and a disulfide anion radical in ribonucleotide reductase (Lawrence *et al* 1999).

The major difficulty arises from the fact that the EPR spectrum is dominated by a strong (>90%) signal of the stable tyrosyl radical cofactor $Y^{\bullet}$, whereas the intermediate species (obtained by freeze quenching of the reaction) provide less than 10% radical yield. At low temperatures, only the spectrum of the stable cofactor is visible; however, the G-resolution permits us to distinguish a weak tail at the low field side indicative for at least another species. To suppress the spectrum of $Y^{\bullet}$, the authors took advantage of the $Y^{\bullet}$ being in the proximity (about 5 Å) of the di-iron cofactor. While the di-iron cluster is diamagnetic at low temperatures, paramagnetic excited states are populated at higher temperatures and the strong dipolar interaction shortens the relaxation of $Y^{\bullet}$. At about 60 K, the signal of $Y^{\bullet}$ is not more detectable in three-pulse echo experiments due to the fast T_1 or T_2 relaxation, and the spectra of the intermediate radicals become visible.

5.4. Relaxation measurements

Pulse methods have a strongly enhanced sensitivity to spin or molecular dynamics, compared with cw-EPR spectroscopy (Millhauser and Freed 1984). This is due to the fact that static broadening mechanisms, which often dominate the line shape of disordered samples, can be suppressed. Additionally, the sensitivity to specific dynamical processes can be tuned by choosing different pulse sequences. Relaxation processes for the coherence and polarization of the electronic spin system depend on the spectral density function $J(\omega)$ of the stochastic process at different frequencies (as $\omega = 0$, ω_{mw}, $2\omega_{\mathrm{mw}}$). If the spectral density of the process is not 'white', the relative contributions at high microwave frequencies will differ from low frequency measurements. Therefore, pulsed HF-EPR will give additional information on the dynamical process and it is especially sensitive to processes on the time scale of the microwave

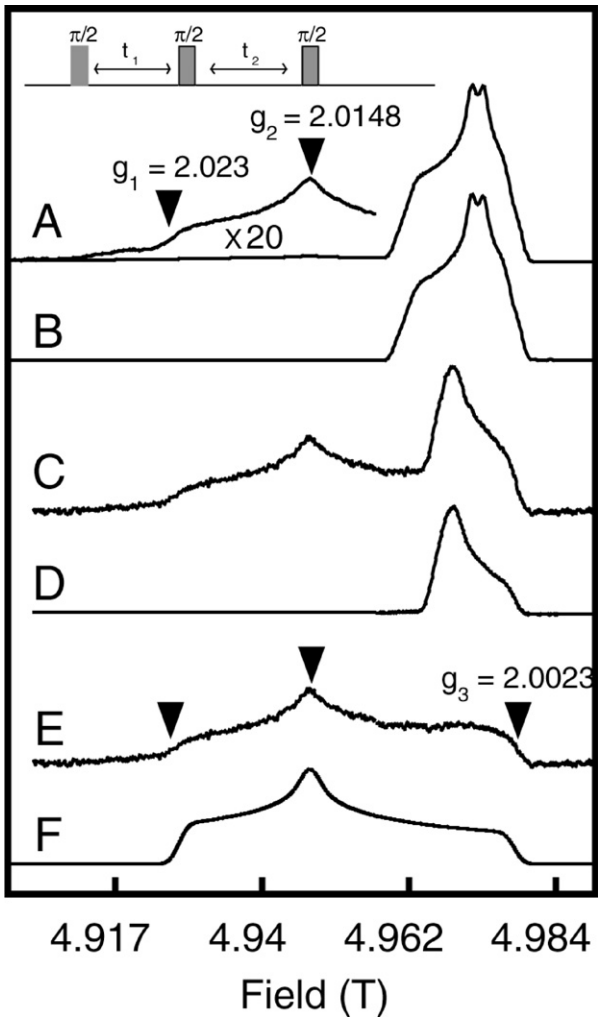

Figure 5. Stimulated echo-detected EPR spectra at 140 GHz of the E441Q R1 RNR reaction, adapted with permission of Lawrence *et al* (1999). (A) Spectra at 10 K after 10 s quenching. (B) Spectrum of $Y^{\bullet}$ for reference. (C) Spectra at 60 K. (D) Reference spectrum at 60 K by quenching after 3 min. (E) Difference spectrum (C)–(D) representing the disulfide radical anion. (F) Simulation of (E).

frequency. Additionally, the orientation selection of HF-EPR spectroscopy, based on the *G*-tensor anisotropy as explained above, allows the measurement of the orientation dependence of the relaxation processes and to investigate the dynamical process in much more detail.

One important mechanism for the relaxation of organic radicals and nitroxides is the modulation of orientation dependent parts of the Hamiltonian by rotational or librational motion of the radical. The anisotropy of the *G*-tensor leads to a dynamic modulation of the Larmor frequency if the molecule changes its orientation with respect to the external magnetic field axis. This leads to an enhancement of the electron transverse relaxation time if this motion occurs on the ps to ns time scale. Because the extent of this dynamical change in Larmor frequency is proportional to the external magnetic field, this effect is more pronounced at high magnetic field values. For protein bound paramagnetic molecules, such as chromophores,

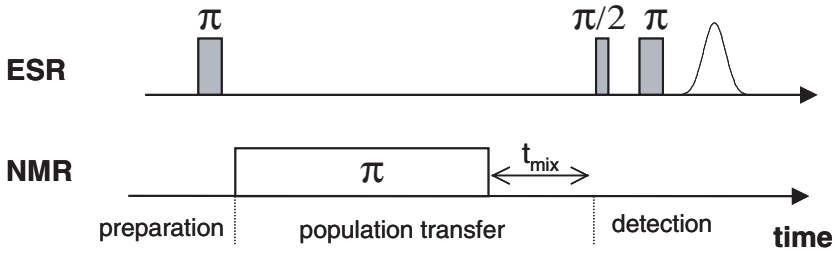

Figure 6. Schematic representation of the Davies ENDOR pulse sequence. Preparation is obtained by a selective microwave π-pulse, whereas the transfer of population from the electron to the nuclear spin manifolds occurs via a selective RF π-pulse followed by a variable mixing time, usually much shorter than the RF-pulse length (Davies 1974).

cofactors or attached spin labels, the motion of the paramagnetic molecule is restricted by sterical effects, covalent or hydrogen bonding to the protein. On the other hand, the overall motion of the protein is too slow, even at room temperature, to contribute to the relaxation processes at high magnetic field values (Borbat *et al* 2001). Therefore, the orientationally selective measurement of the relaxation times caused by this librational modulation allows a detailed picture of the motion to be obtained (Prisner 2004).

6. Pulsed ENDOR

ENDOR is a method that allows the determination of the hyperfine coupling between electron and nuclear spins, giving insight into the nature and the number of nuclear spins coupled to a paramagnetic species, and particularly into their inter-spin distances. ENDOR has become a very valuable tool for structural studies of biological systems involving active site paramagnetic centres, such as metal binding sites, metal clusters and amino acid cofactors, as it permits us to investigate functional intermediate states under biologically relevant conditions. Several examples on the application of high field ENDOR will be illustrated in section 7.

In contrast to conventional EPR, ENDOR directly detects the hyperfine transitions of the nuclei coupled to the electron spin (figure 1) by transferring population between the higher polarized electron Zeeman and the weaker polarized nuclear Zeeman spin manifolds. The ENDOR technique becomes considerably advantageous at high magnetic fields ($B > 1$ T) because it relies on the subsequent excitation of only allowed EPR and NMR transitions. The Davies ENDOR sequence is illustrated in figure 6.

However, because technical issues render the implementation of pulsed ENDOR quite challenging, only a few HF-ENDOR spectrometers operate currently at 95 GHz (Burghaus *et al* 1992, Disselhorst *et al* 1995, Rohrer *et al* 1995, Gromov *et al* 1999), 140 GHz (Bennati *et al* 1999a), 180 GHz (Hertel *et al* 2004) and 270 GHz (Blok *et al* 2004a). Nevertheless, the first prototype of a commercial (Bruker EPR Division 2000) high frequency ENDOR probe has become available, opening new perspectives for the applications of ENDOR techniques. The most important aspects of high field ENDOR spectroscopy will be analysed in more detail in the following section.

6.1. Technical aspects

The major technical challenge in ENDOR at high frequencies is related to the requirement of a concomitant microwave and radio frequency (RF) irradiation at the sample. The reduced size

of the cylindrical resonator, customarily employed in HF-EPR spectrometers at frequencies below 300 GHz, does not allow an NMR RF coil to be mounted inside the resonator. An external RF coil, however, suffers from a dramatic loss of RF magnetic field strength at the sample position (RF skin depth in silver at 200 MHz $\approx$4 μm). A partial solution of the problem has been achieved by inserting slots in the cavity along the cylinder walls perpendicular to the cavity z-axis (Burghaus *et al* 1992). With this design, pulse lengths of the order of 10–20 μs can be achieved with a tuned RF-circuit at medium power levels (400 W) (Bennati *et al* 1999a) or with a broad band circuit at high RF power (1–2 kW) (Gromov *et al* 1999). More recently, a new resonator design has been proposed (Weis *et al* 1999) where the cavity wall is replaced by a flat wire forming the RF coil, thus circumventing the issue of RF penetration and allowing for both high MW and RF irradiation efficiency. A similar design has also been adopted by Bruker Analytik (Höfer, private communication).

Other technical issues are related to the requirements of performing large (>5 MHz) RF sweeps at variable frequency ranges and with constant RF power. Particularly, the matching behaviour becomes increasingly critical towards higher frequencies. This, combined with the intrinsic frequency dependence of the RF output power of commercial amplifiers can lead to artefacts in ENDOR spectra, in particular baseline drifts and asymmetries of the lines at low temperatures. To improve the performance, random excitation and acquisition have been recently proposed rather than a sequential variation of RF frequencies (Epel *et al* 2003).

6.2. Zeeman resolution

When approaching the so-called high field condition ($H_Z^I \gg H_A^I$), ENDOR spectra substantially simplify because nuclear spins become quantized along the external magnetic field and the two hyperfine transitions $\nu_\pm$ connected to the two electron spin manifolds $\pm m_S$ are centred around the nuclear Zeeman frequency ν_L according to

$$\nu_\pm = |\nu_L \pm m_S A_{zz}^i|, \tag{15}$$

where A_{zz}^i is the angular dependent hyperfine coupling associated with nucleus i. The negligibility of non-secular terms affects not only the resonance frequencies but also the transition probabilities and thus the intensities of the ENDOR lines. Whereas at low fields, transition probabilities depend on the size and anisotropy of the hyperfine couplings (Dalton and Kwiram 1972), in the high field limit they approach unity and hyperfine spectra are symmetric around the nuclear Zeeman frequency. These features considerably simplify the interpretation of the spectra and often hyperfine parameters can be extracted from data without spectral simulation.

One example, which illustrates the Zeeman resolution of ENDOR spectra at high fields, consists of the 94 GHz ^{17}O-ENDOR spectrum of $H_2^{17}O$ ligated water in the Ras·Mn^{2+}·GDP complex (figure 7). Here, the $S = \frac{5}{2}$ high spin of the Mn^{2+} ion and of the ^{17}O nucleus introduce some layers of complexity into the ENDOR spectrum: whereas the Mn^{2+} $S = \frac{5}{2}$ spin generates hyperfine multiplets according to the different m_S states in equation (15), the ^{17}O $I = \frac{5}{2}$ quadrupole nucleus splits the hyperfine line according to the different nuclear states:

$$\nu_\pm(m_I) = |\nu_L \pm m_S A_{zz}^i + 3Q_{zz}^i(2m_I - 1)|, \tag{16}$$

where Q_{zz}^i is the angular dependent quadrupole tensor component of nucleus i. However, at 95 GHz, an almost selective EPR excitation of the electron spin $m_S = \pm\frac{1}{2}$ manifolds is feasible (section 4.3). Further, the nuclear Zeeman frequency of ^{17}O ($\nu_L = 20.2$ MHz at 3.5 T) is well separated from other low-gamma nuclei, which may be observable in natural abundance in proteins (^{13}C, ^{14}N). Finally, the ENDOR resonances become symmetric

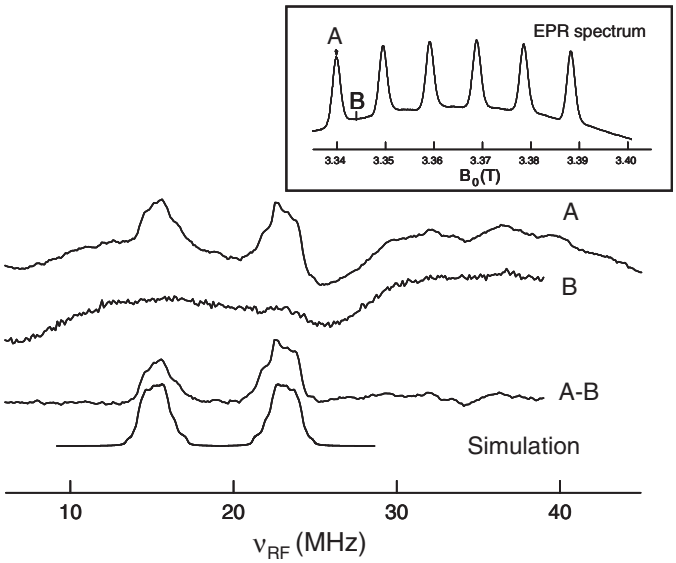

Figure 7. 94 GHz ^{17}O Davies ENDOR spectrum of the wild-type Ras·Mn^{2+}·GDP complex. A: With excitation on the $m_S = \pm\frac{1}{2}$ transition. B: Excitation outside the $m_S = \pm\frac{1}{2}$ transition (see EPR spectrum in the inset). C: Difference spectrum (A–B) to eliminate baseline distortions and contributions from higher electron spin manifolds. D: Simulation of C within the high field approximation with the parameters given in the text.

around the nuclear Zeeman frequency and the quadrupole multiplets are clearly resolved. A simulation of the spectrum in figure 7 is straightforward in the high field limit and the obtained hyperfine and quadrupole tensor principal axis values ($A_x = |6.27|$ MHz, $A_y = |6.86|$ MHz, $A_z = |10.1|$ MHz, $Q_x = -0.238$ MHz, $Q_y = 0.238$ MHz, $Q_z = 0$ with interconnecting Euler angles $\alpha = 15^\circ$, $\beta = 35^\circ$, $\gamma = 0$) are in good agreement with X-band ESEEM and ENDOR on the Mn^{2+} aqua-complex (Tan *et al* 1994).

6.3. Orientational selectivity

Information about the mutual orientation of the G and hyperfine tensors can be obtained in a so-called orientational selective ENDOR experiment, where hyperfine spectra are correlated with the EPR resonance field (Rist and Hyde 1970). In orientational selective ENDOR, hyperfine spectra result only from molecular orientations excited within the microwave pulse bandwidth, which is typically much smaller than the total width of the EPR powder pattern. When the EPR line is dominated by G-anisotropy, a set of ENDOR spectra recorded through the EPR line leads to characteristic two-dimensional patterns that correlate hyperfine and G-tensors, a technique that has been well exploited at X-band and Q-band EPR frequencies (Rist and Hyde 1970, Hoffman *et al* 1984) on transition metal ion complexes. For organic radicals (in particular protein radicals) with small G-anisotropy ($\Delta g/g < 1\%$) the method becomes accessible only at high magnetic fields.

First orientational selective high field ENDOR spectra of organic radicals were reported by Rohrer at 95 GHz for plastoquinones (Rohrer *et al* 1995) and for ubisemiquinone in bacterial reaction centres (Rohrer *et al* 1998) and by Bennati (Bennati *et al* 1999a) and Bar (Bar *et al* 2001) at 140 GHz for the tyrosyl radical ($Y^\bullet$) in ribonucleotide reductase. Since two-dimensional powder patterns confer substantial restrictions on spectral simulations,

orientational selectivity also improves the precision in the assignment of lines in complex ENDOR spectra with more than one nucleus.

Very recently, orientational selectivity was demonstrated at the W-band in combination with two-dimensional TRIPLE spectroscopy (Goldfarb *et al* 2004). Analysis of the shapes of the cross-peaks in a two-dimensional TRIPLE experiment showed that these are highly dependent on the orientation of the hyperfine tensors of the two nuclei contributing to this particular peak. Accordingly, orientational selectivity contributes to simplify the information content, as was demonstrated with the analysis of a Cu(II)-bis(2, 2′ : 6′, 2″ terpyridine) complex.

6.4. Polarization effects

Under certain experimental conditions, high field ENDOR spectra display the appearance of asymmetric or negative ENDOR lines. This observation turned out to be very useful because the polarization pattern provides a means to directly determine the absolute sign of the hyperfine coupling. The observation of polarized high field ENDOR spectra was initially reported in studies where relatively long RF pulses were used (Goldfarb *et al* 1996, Bennebroek and Schmidt 1997). Bennebroek and Schmidt (Bennebroek and Schmidt 1997) attributed this effect to the high thermal electron spin polarization at high microwave frequencies ($\nu \geqslant 95$ GHz) and very low temperatures (typically $T < 10$ K) in combination with an electron spin-lattice relaxation time, T_{1e}, that is shorter than the total mixing time (t_{mix}, spacing between the RF and the detection pulses, see figure 6). In the case of an electron spin $S = \frac{1}{2}$ coupled to a nuclear spin with positive g-factor, this results in a negative ENDOR effect for lines belonging to the $m_S = -\frac{1}{2}$ manifold and a positive one for the lines in the $m_S = +\frac{1}{2}$ manifold.

Later on, asymmetric ENDOR spectra were reported also during Davies ENDOR experiments under rather 'standard conditions' (Manikandan *et al* 2001), i.e. $t_{mix} \ll T_{1e}$ and $T_{1e} \ll t_R \ll T_{1N}$, T_{1x} with t_R being the shot repetition time, and T_{1N} and T_{1x} the nuclear and cross relaxation times, respectively. The observation lead Epel *et al* (2000) to extend the model of Bennebroek and Schmidt to consider all possible relaxation pathways during the ENDOR experiment, specifically the role of the nuclear and cross relaxations T_{1N} and T_{1x}. The results showed that for these so-called 'standard conditions', asymmetries in the ENDOR lines occur as a consequence of the saturation of the nuclear transitions at very long T_{1N} and T_{1x}. In this case, the polarization of the ENDOR signal is opposite as in the case analysed by Bennebroek and Schmidt, i.e. for a positive A and g-factor the lines in the $m_S = +\frac{1}{2}$ manifolds are positive and those of the $m_S = -\frac{1}{2}$ manifolds are negative. The model provided a good description for experimental ^{1}H-ENDOR data recorded on Cu(II)histidine and Cu(II)Imidazol complexes in frozen aqueous solutions.

Interestingly, polarization effects have not been reported so far on any investigated frozen solution of organic amino acid radicals but rather in conjunction with ENDOR on metal centres or metal clusters. Very recently, completely polarized ENDOR spectra under 'standard conditions' were reported in a ^{57}Fe ENDOR study of a 4Fe4S cluster (Bennati *et al* 2004b). Application of the model by Epel *et al* leads to a prediction of the sign of the four ^{57}Fe hyperfine couplings well in agreement with predictions from Mössbauer experiments.

Finally, high thermal electron spin polarization allows the determination of the sign of the hyperfine couplings in high spin systems. This was demonstrated by Manikandan *et al* (Manikandan *et al* 2000) in the investigation of the manganese-binding site of concanavalin A. In a high-spin system such as the $S = \frac{5}{2}$ of the Mn^{2+} ion with a weak ZFS, selective excitation of either transition associated with the higher electron spin manifolds $\pm\frac{3}{2}$ and $\pm\frac{5}{2}$, leads to asymmetric ENDOR patterns. For a positive hyperfine coupling and a positive g-factor, the ENDOR line associated with the lowest electron spin manifold occurs at the high field side.

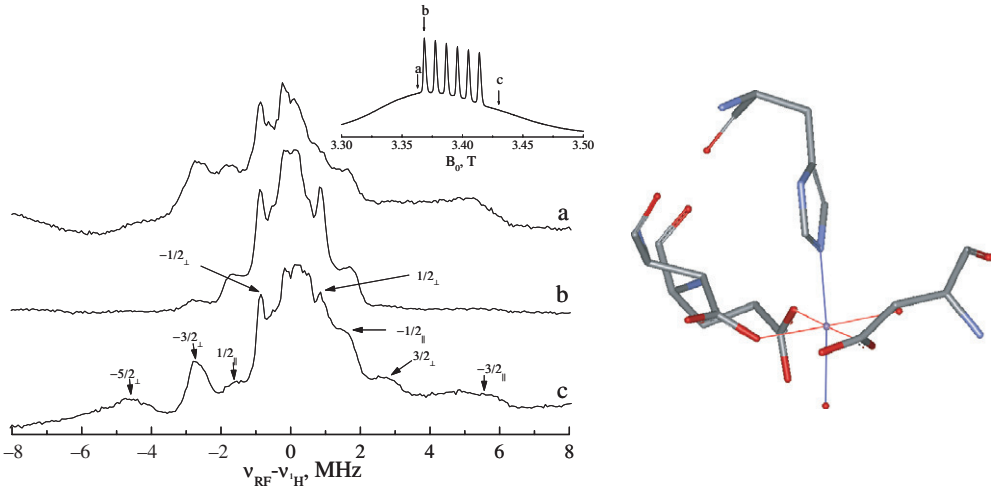

Figure 8. (Right) The structure of the Mn^{2+} binding site in concanavalin A and (left) ^{1}H Davies ENDOR spectra of frozen solution (4–5 K) of concanavalin A in 40% glycerol-d_3 and D_2O buffer; reproduced with permission from Goldfarb and Arieli (2004). The inset shows the excitation positions in the EPR spectrum.

The method is illustrated in figure 8, where the ^{1}H-ENDOR spectra of concanavalin A in D_2O solution are represented for three different selective excitations.

The spectrum recorded at position (a) mainly arises from the $|-\frac{3}{2}\rangle \rightarrow |-\frac{1}{2}\rangle$ electronic transition and clearly displays the $A_{||}$ and $A_{\perp}$ features of the $m_S = -\frac{1}{2}$ and $-\frac{3}{2}$ manifolds, indicating that $A_{||} > 0$ and $A_{\perp} < 0$. Spectrum (c) also shows ENDOR signals from the $m_S = \frac{1}{2}$ and $\frac{3}{2}$ manifolds and spectrum (b) obtained from excitation of the $|-\frac{1}{2}\rangle \rightarrow |\frac{1}{2}\rangle$ electron spin manifold is instead symmetric as expected.

7. Applications in structural biology

Despite the fact that the technical developments have only recently reached a level where HF-EPR spectroscopy can be routinely performed, the number of papers on its application in structural biology is increasing exponentially. In many studies, a combination of EPR and other spectroscopical, structural or biochemical methods have been applied to characterize proteins. We will concentrate in this last section mainly on new publications where HF-EPR contributed substantially to the understanding of the results and therefore will not give a comprehensive citation of all applications in this area.

7.1. Photosynthetic proteins

In photosynthetic proteins a photo-initiated electron transfer reaction occurs, that creates transient paramagnetic species, which can be trapped and chemically stabilized. The sequential order, energetics, spectral properties and their interplay and arrangement have been characterized extensively by many EPR spectroscopists since the 1960s (Hoff 1979). Later on, the bacterial photosynthetic reaction centre of *Rhod. viridis* was the first membrane bound protein crystallized (Michel 1982) and characterized by x-ray diffraction (Deisenhofer *et al* 1986) to obtain a high resolution structure. This allowed the placement of the organic cofactor skeleton into the full protein structure and to address much more specific structural

and functional questions with specific point mutants and advanced EPR spectroscopy. It also served as a benchmark system for biological EPR spectroscopy, where many of the new methods were first applied. HF-EPR helped to gain new insights, because for the first time the main G-tensor values of these cofactors could be accurately measured. Differences in the G-tensor values between various organisms, on specific point mutations and in comparison to model systems permitted us to draw, together with DFT quantum theoretical calculations (Kaupp 2002), conclusions on the specific binding geometry of the cofactors in the proteins.

7.1.1. G-tensors of organic cofactors. For the first electron donor molecule P^{+}_{700} of photosystem I, a chlorophyll dimer, the G-tensor values have been determined for the first time by cw HF-EPR at 140 GHz (Prisner *et al* 1993) in a deuterated sample from *Synechococcus lividus*. At higher frequencies (330 GHz) the same G-tensor values were reported for protonated samples (with larger inhomogeneous linewidths) from spinach (Bratt *et al* 1997). Measurements on mutations of the axial ligand of one of the chlorophylls in *C. reinhardtii* showed a change in the G_{zz} component of the G-tensor, while no changes where observed for the mutation at the second chlorophyll molecule (Petrenko *et al* 2004). This was interpreted in terms of an asymmetric spin density on the two chlorophyll molecules in the dimer and a nonplanar structure of one of the chlorophylls. The same type of measurements has been performed on $P^{+\bullet}_{865}$ of bacterial reaction centres from *Rhod. spheroides* on a small single crystal (Klette *et al* 1993). This allowed the determination of not only the main G-tensor values but also their relative orientation with respect to the molecular axis system. The same main values were reported for frozen solution samples at higher microwave frequencies (360 GHz) (Bratt *et al* 1999). Measurements on mutants of the axial histidine ligand showed changes in the anisotropy of the G-values measured at 360 GHz and were interpreted with structural changes of the acetyl group attached to the spin-carrying bacteriochlorophyll-*a* half of the dimer (Fuchs *et al* 2003). A substantially less anisotropic G-tensor was observed for $P^{+\bullet}_{960}$ of a bacteriochlorophyll-*b* containing reaction centre from *Bc. viridis*, which could only be resolved at 670 GHz microwave frequency and 24 T magnetic field strength (Bratt *et al* 2003). HF-EPR measurements performed on the triplet state of the chlorophyll dimer molecule allowed the extraction of the G-tensor values of this molecular state from the spectra, which are dominated by the strong ZFS interaction of the two unpaired electron spins (Pashenko *et al* 2001). The G-tensor anisotropy leads to spectra that are no more antisymmetric to their centre. Differences in the main G-tensor values compared to the cation state of the dimer could be interpreted by singlet–triplet spin-orbit coupling to a close lying excited singlet state or by a redistribution of the unpaired electron over the two dimer halves (Labahn and Huber 2001, Zeng *et al* 2003). In the same way the temperature dependence of the triplet state G-tensor values could be attributed to singlet–triplet spin-orbit coupling or to small structural changes upon freezing (Zeng and Budil 2003).

The same type of experiments were performed for the different electron acceptor anion radicals generated in the electron transfer reaction. In photosystem II of *C. reinhardtii*, the intermediate pheophytin electron acceptor was measured at 280 GHz for several mutants (Dorlet *et al* 2001). The shifts in the g_x component of the different point mutants could be related to the hydrogen bonding capacity of the respective amino acids to the pheophytin radical.

The next electron acceptor molecules in photosynthetic proteins are quinones. In some cases their G-tensor values can already be resolved at Q-band frequencies (34 GHz), especially in deuterated samples and single crystals. Nevertheless, a more detailed determination of these values and their subtle changes on mutation were only observable by HF-EPR spectroscopy, and build the basis of a detailed quantum theoretical investigation of the G-tensor dependence on the hydrogen bonding network of the quinone cofactor (Kaupp *et al* 2002). The experimental

HF-EPR determination the G-tensors of semiquinone radicals in bacterial reaction centres, photosystem I and II are already reported in two review articles (Stehlik and Möbius 1997) (Lubitz and Feher 1999) and short overview articles on photosystem I (Teutloff *et al* 2001) and photosystem II cofactor radicals (Un *et al* 2001a).

Similarly, HF-EPR spectroscopy was used to determine the main g-values of other cofactors in photosynthetic proteins. The g-values of carotenoid and chlorophyll-z were determined at 130 GHz in photosystem II of deuterated *Synechoc. Lividus* (Lakshmi *et al* 2000) and at 280 GHz in spinach (Faller *et al* 2000). In the latter case, the one-dimensional ordering of the membranes dried on plastic films allowed the orientation of the chlorophyll-z plane normal to the membrane surface to be obtained. The ordering of membranes on two-dimensional films were also combined with HF-EPR spectroscopy to obtain orientational information of the tyrosyl radical Y_D and the electron acceptor semiquinone radical Q_A^- in photosystem II (Dorlet *et al* 2000) and of the first electron acceptor semiquinone molecule A_1^- in photosystem I (Fuhs *et al* 2002; MacMillan *et al* 1997). In the same spirit, the ordering of whole cells in high magnetic fields have been observed by HF-EPR in photosystem I preparations (Heinen *et al* 2004).

The G-anisotropy is a sensitive probe of the spin density distribution over the molecule and is influenced by the hydrogen bonding to the protein pocket and electrostatic effects of the close surrounding. The very accurate measurement of these values by HF-EPR provided, on the one hand, the benchmarks for quantum chemical calculations and allowed the correlation of on the other hand, for the first time, the observed values to structural details of the cofactor binding pocket. Whereas semiquinone radicals have been already thoroughly investigated by quantum chemical density functional calculations (Kacprzak and Kaupp 2004), this is still demanding for larger molecules like chlorophylls or even chlorophyll dimers. Nevertheless, the shifts in the g-values upon mutation can be empirically related to structural aspects, such as the hydrogen bonding of the cofactors. Finally, HF-EPR spectroscopy allowed the unambiguous distinguishing, for the first time, of the EPR signals of these aromatic organic cofactors and therefore these cw HF-EPR spectra represent a 'fingerprint' to assign the respective radicals. This is nicely shown in figure 9, where the 285 GHz HF-EPR spectra of different cofactor radicals in PS II are depicted on a g-value axis. The various species can be clearly distinguished and also differences in the local electrostatic surrounding (as shown for tyrosyl radicals) can be sensitively monitored (Un *et al* 2001a).

7.1.2. Correlated radical pairs. The spectral resolution of the main G-tensor values of the semiquinone radicals, which are the primary electron acceptors in the light driven electron transfer reactions, allows very detailed information on the charge separated radical pairs created transiently after flash photoexcitation to be obtained. The two spins of the donor–acceptor radical pair are created from a singlet excited state and are coupled to each other through a space magnetic dipole–dipole interaction. Therefore, highly spin polarized absorptive-emissive spectra are observed, which contain information about the relative orientation of the donor and acceptor molecules (Stehlik *et al* 1989). The extraction of this structural information is hampered at lower microwave frequencies by unresolved hyperfine interactions obscuring the spin polarized spectra. At high magnetic field values, the spectra are dominated by the anisotropic G-tensor and the information on the dipolar coupling, such as the distance and the relative orientation of the two paramagnetic molecules, can be more easily determined (Stehlik and Möbius 1997). This was first demonstrated for the bacterial reaction centre R26 of *Rhod. sphaeroides* (Prisner *et al* 1995), where these measurements gave the relative orientation of the two cofactors P_{865}^+–Q_A^- in agreement with the x-ray structural data. Additionally, they allowed the resolution of the ambiguity of the G-tensor axis orientation of the primary donor P_{865}^+ with

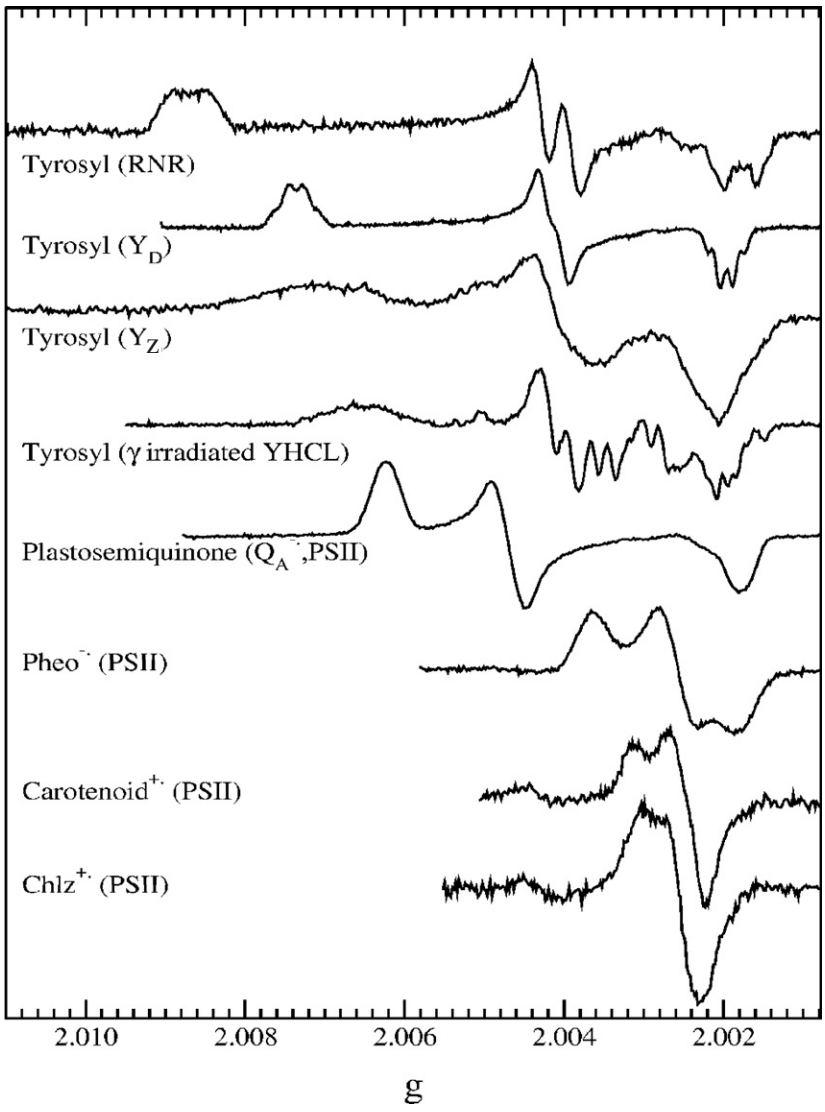

Figure 9. HF-EPR spectra of radicals in PSII and comparison with the tyrosyl radical in RNR, adapted with permission of Un *et al* (2001a). All spectra were recorded at 285 GHz with the exception of the Y_Z spectrum, which was recorded at 245 GHz.

respect to the molecular axis system left from single crystal cw HF-EPR studies (Klette *et al* 1993). The same experiments were performed on photosystem I to determine the relative orientation of the spin-correlated radical pair P_{700}^{+}–A_1^{-} (van der Est *et al* 1997). Pulsed HF saturation recovery experiments have been used to obtain information on the location of the chlorophyll Chl^{+} and the carotenoid Car^{+} radicals created in photosystem II, when the primary electron transfer pathway is inhibited (Lakshmi *et al* 2003). The magnetic dipolar coupling to the non-haeme iron can be quenched by treatment with cyanide, which changes the high spin $S = 2$ state of the iron into the low-spin $S = 0$ state. The loss of dipolar relaxation could be measured selectively for both radical pairs Chl^{+}–Fe(II) and Car^{+}–Fe(II) at 5 T field strength, because the two organic cofactors are spectrally separated.

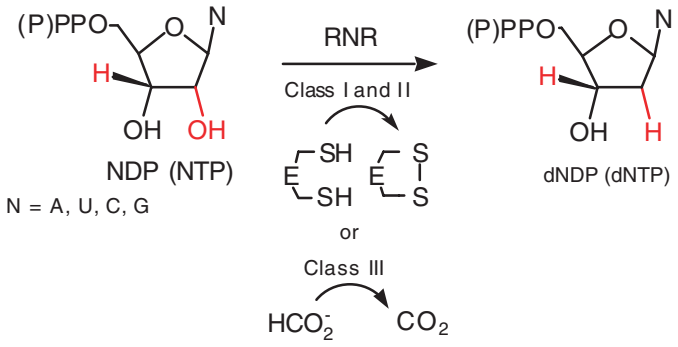

Figure 10. Reaction scheme of ribonucleotide reductase classes I, II and III.

7.1.3. Orientation selective ENDOR. Orientation selective ENDOR experiments have been performed on the semiquinone radicals Q_A and Q_B of bacterial reaction centres R26 of *Rhod. sphaeroides* (Rohrer *et al* 1998). These measurements provided the orientation and distance of the hydrogen bonds from the semiquinones to the protein. Pulsed ENDOR was also performed on the photoexcited spin-correlated radical pairs, resulting in highly polarized hyperfine spectra (Bittl and Zech 2001). In combination with high fields, this again allows orientation selected information to be obtained and disentangle the complicated polarized hyperfine lines. The method has been recently applied to bacterial reaction centres from *Rhod. sphaeroides* (Poluektov *et al* 2004) and differences in the hyperfine couplings of the photogenerated radical with respect to the chemical reduced semiquinone radical were observed.

7.1.4. Librational dynamics of semiquinones. The orientation selection can also be used to measure the anisotropic small angle librational motion of the protein bound cofactors at low temperatures. This librational motion induces relaxation of the unpaired electron spin if the motion occurs on a time scale of nanoseconds (transversal relaxation) or on the time scale of the inverse microwave frequency (longitudinal relaxation). The first case was observed for the Q_A^- (Rohrer *et al* 1996) and Q_B^- (Schnegg *et al* 2002) radicals in bacterial reaction centres at temperatures between 100 and 190 K. The strong relaxation anisotropy was explained by an anisotropic librational tumbling of the semiquinone radical on a cone around its C–O axis. This motion is different from the librational motion of the same semiquinone molecule in frozen isopropanol solution and was interpreted as restricted by the hydrogen bonding of the cofactor to the protein (Prisner 2004).

7.2. Ribonucleotide reductase

Ribonucleotide reductase (RNR) is the prototype radical enzyme that catalyses the conversion of nucleotides to deoxynucleotides in all living cells, the rate determining step in DNA biosynthesis (Jordan and Reichard 1998). The reaction scheme is illustrated in figure 10.

Since the discovery of the catalytically essential tyrosyl radical in Class I RNR by EPR spectroscopy, RNRs have provided a paradigm for thinking about the role of amino acid radicals and substrate derived radicals in biological catalysis and for identification of protein and substrate radical intermediates using time resolved and high field EPR methods (Stubbe and van der Donk 1998). RNRs have been divided into four classes based on the radical/metallo cofactors essential for catalysis. It has been proposed that in all classes the function of each cofactor is to generate a transient thiyl radical that initiates a radical dependent nucleotide reduction.

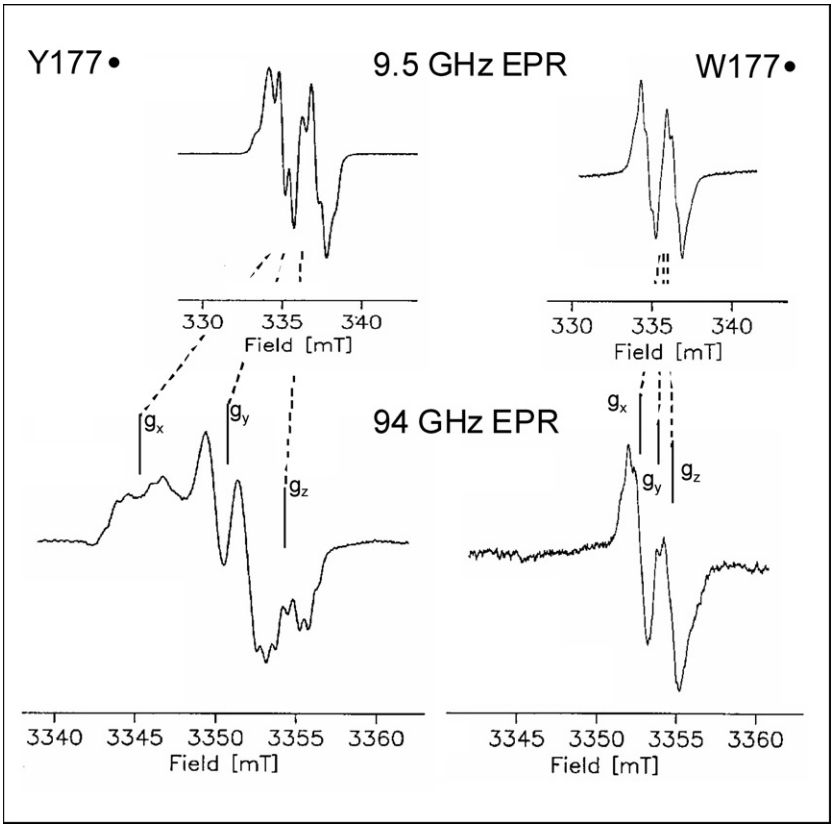

Figure 11. Comparison of X-band and W-band EPR spectra of the tyrosyl radical Y177• in *mouse* R2 (left) and of the tryptophan radical W177• in the *mouse* mutant Y177W (right); reproduced with permission from Bleifuss *et al* (2001).

7.2.1. The essential tyrosyl radical in Class I RNR R2. The first high-frequency EPR spectrum of the essential tyrosyl radical (Y•) in the R2 subunit of Class I RNR from *E. coli* was reported by Gerfen *et al* (1993) at 140 GHz. Subsequently, high frequency EPR spectra of Y• from RNRs in other organisms and mutants were recorded by several authors, as has been summarized in a recent review article (Bennati *et al* 2001). The HF-EPR powder line shape of Y• is dominated by the anisotropy of the G-tensor with g-values found as typical for tyrosyl radicals. A typical high field (95 GHz) spectrum of Y• from the mouse organism is displayed in figure 11. The ∼20 G splitting visible in the centre of the spectrum is due to a large hyperfine coupling of one β-methylene proton. On the edges of the powder pattern, the hyperfine coupling with the three- and five-ring protons is greatly resolved. The hyperfine coupling is not observed in the centre of the powder pattern ($B||g_y$), according to an anisotropic hyperfine tensor of the type $A_x > A_z \gg A_y$. The g_x value has been found to vary and reflect stabilization of the non-bonding orbitals of the oxygen of the radical through electrostatic and hydrogen-bonding interactions (Un *et al* 1995). This hypothesis has been supported by ENDOR investigations at 35 and 140 GHz on D_2O exchanged R2 proteins (van Dam *et al* 1998, Bar *et al* 2001). Additionally, high frequency 140 GHz pulsed ENDOR of Y• allowed the resolution and unambiguous assignment of the small hyperfine couplings of the ring protons (Bennati *et al* 1999a). Recently, high frequency (95 GHz) EPR experiments were performed on oxidized single crystals of R2 (Högbom *et al* 2003). From the rotation pattern of the

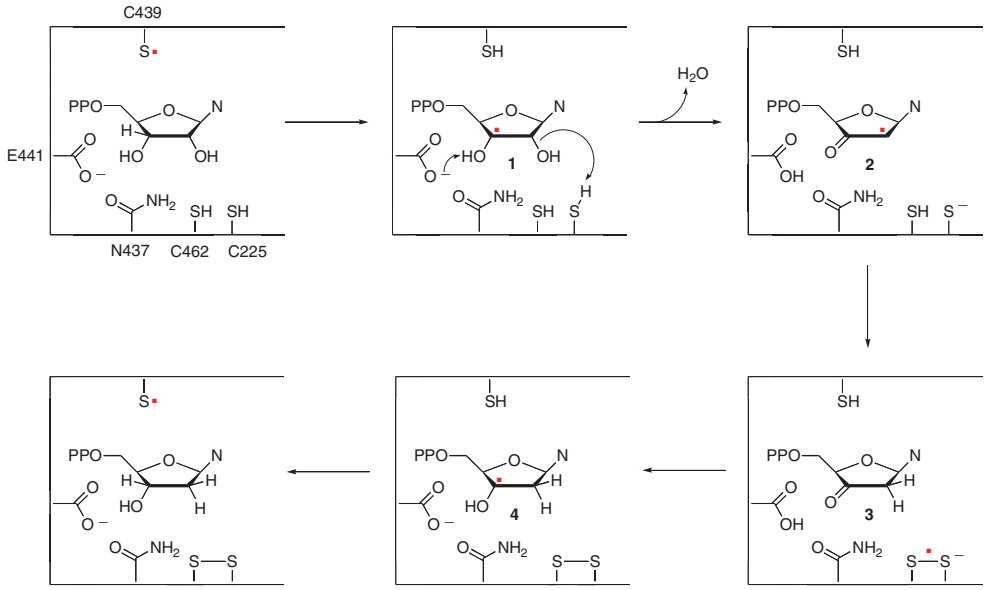

Figure 12. Proposed model for the reduction process of ribonucleotides with RNR (Stubbe and van der Donk 1998).

spectra, the orientation of the radical was determined in the crystal frame. Comparison with the crystal structure, where Y122 is reduced, revealed a displacement of the radical from the metallo-cofactor, which may lead to implications for the mechanism of radical transfer from R2 to R1.

In mutants of R2 from *E. coli* and mouse, where the essential tyrosyl radicals were mutated into a phenylalanine Y122F (*E. coli*) and into a tryptophan Y177W (mouse), respectively, new neutral tryptophan radicals were also observed (Bleifuss *et al* 2001). Despite the strong similarities of the X-band spectra, these radicals can be spectroscopically clearly distinguished from $Y^{\bullet}$ at high frequencies, as displayed in figure 11. In a Y122H mutant of *E. coli* R2, 95 GHz EPR and $^{1}H/^{2}H$- and ^{57}Fe ENDOR spectroscopy allowed the identification of a new $Fe^{3+}Fe^{3+}$ centre strongly coupled to one radical in the vicinity (Kolberg *et al* 2000).

7.2.2. Mechanistic studies of RNR inhibition. To better illustrate the HF-EPR studies on RNR inhibitors and mutants, the proposed model for the reduction process is presented in figure 12. In class I and class II, four amino acid residues are essential for the reduction mechanism. One cysteine (Cys 439, *E. coli* numbering) provides the thiyl radical as initiator, two additional cysteines, Cys225 and Cys 462, deliver the reducing equivalents, and a glutamate, E441, assists in ketyl radical formation and allows the reduction of the 3′-ketodeoxynucleotide (step 4) via a disulfide radical anion. Without discussing the chemistry of the RNR mechanism in detail, it is nevertheless important to realize that all proposed steps in figure 12 involve radical chemistry and, therefore, EPR spectroscopy is an ideal tool for the identification of the proposed intermediates.

Two approaches have been used successfully to study the nucleotide reduction mechanism. One consists of using substrate analogues as mechanism-based radical traps and the second uses site-directed protein mutants. Both result in the generation of long-lived (second timescale) radical intermediates amenable to high frequency EPR spectroscopy. Direct evidence for

the first chemical step in nucleotide reduction (the abstraction of the 3′-hydrogen from the nucleotide) was achieved using the mechanism based inhibitor 2′-(fluoromethylene)-2′-deoxycytidine 5′-diphosphate (FMCDP) (Gerfen *et al* 1998). The reaction leads to the generation of a new substrate derived radical in the active site of the R1 subunit. The combination of 140 and 9 GHz EPR established the g-values and the hyperfine couplings of the signal, which are consistent with an allyl radical, in which the fluorine atoms have been replaced with an active site residue. Identification of this radical permitted us to derive the chemical mechanism of deactivation. Another mechanism based inhibitor, 2′-azido-2′-deoxyuridine 5′-diphosphate (N_3UDP) has recently provided the first evidence for the postulated 3′-ketodeoxynucleotide in the reduction process. The reaction of N_3UDP with RNR generates in the active site a radical stable on time scales of a minute. Previous 140 and 9 GHz EPR experiments in combination with ^{2}H and ^{15}N isotope labelling had led to the assignment of this species to a nitrogen centred radical covalently attached to a cysteine in the active site (van der Donk *et al* 1995). Very recent 9 and 140 GHz experiments with 3′–[^{17}O]–N_3UDP in combination with DFT calculations allowed the establishment of the structure of this radical, in which Cys225 is linked to the 3′-carbon of the nucleotide through the nitrogen atom (Cys–S–N$^\bullet$–3′C–) (Bennati *et al* 2004a).

Finally, the use of time domain 140 GHz spectroscopy on a E441Q mutant of RNR allowed the isolation of the first radical intermediate on the direct pathway of nucleotide reduction, the disulfide radical anion (Lawrence *et al* 1999). These 140 GHz spectra have been discussed in section 5.3 and displayed in figure 5.

7.2.3. The glycyl radical in class III RNR. The anaerobic class III RNR together with two other enzymes, the pyruvate formate lyase (PFL) and the benzylsuccinate synthase (BSS), all of them in anaerobically grown micro-organisms, have been found to carry a dioxygen-sensitive glycyl radical. For the first two systems, the three-dimensional structures have revealed that the radical is at the active site and is expected to play an essential role during initiation of the catalysis. On the basis of the sequence homologies at the glycine sites, it is very likely that a much larger number of enzymatic systems depend on a glycyl radical for activity (Selmer and Andrei 2001). Whereas the X-band EPR spectra are dominated by an isotropic hyperfine coupling to the α-proton, the g-values were recently resolved at 285 and 525 GHz (Duboc-Toia *et al* 2003). The G-anisotropy is very small ($\Delta(g_z - g_x) = 0.0019$–$0.0023$) as expected for carbon-centred radicals. On the other hand, a much higher field was required to separate g_x and g_y in PFL and BSS, which might reflect small differences in the electrostatic environment along the respective directions.

7.3. Other radical enzymes

In the past decade, a number of important radical dependent enzymes have been discovered and the involved radical species have been identified predominantly by EPR spectroscopy (Stubbe and van der Donk 1998). The recent widespread use of HF-EPR techniques allowed a much more precise characterization of these species and some representative studies are summarized in the following.

Besides Class I RNR and the photosynthetic reaction centres, amino acid or cofactor radicals were characterized with high frequency EPR in galactose oxidase (Gerfen *et al* 1996), prostaglandin H_2 synthase-1 (Dorlet *et al* 2002), cytochrome c peroxidase (Ivancich *et al* 2001), catalase-peroxidase (Ivancich *et al* 2003), P450cam (Schünemann *et al* 2004), DNA photolyase (Fuchs *et al* 2002) and quinoproteins alcohol dehydrogenases (Kay *et al* 2004). In galactose oxidase, the protein-based radical is antiferromagnetically coupled to a copper ion,

but the free radical can be generated by chemical oxidation of the apoenzyme and is localized on a cross-linked tyrosine–cysteine residue. The high frequency EPR results (Gerfen *et al* 1996) lead to the hypothesis that the spin density distribution is interestingly localized on the tyrosine–cysteine moiety rather than on the tyrosine π-system, in contrast to tyrosyl radicals.

Various tyrosyl radicals generated by reaction of both native and indomethacin-inhibited ovine prostaglandin H_2 synthase-1 with hydrogen peroxide were recently examined at 130, 190 and 285 GHz with EPR spectroscopy (Dorlet *et al* 2002). The spectra of the initially formed tyrosyl radical, of the species formed after subsequent incubation at 273 K and of the indomethacin-inhibited enzyme all reveal typical g-values for tyrosyl radicals but with a wide distribution in g_x, indicative of hydrogen bonded species. The high field observations are consistent with a model in which the tyrosyl phenyl ring rotates with respect to both the protein backbone and the putative hydrogen bond donor during evolution of the initial signal to the subsequent species.

A common property of peroxidases and catalases is the formation of a highly oxidizing paramagnetic intermediate, the so-called Compound I, which consists of an oxoferryl moiety, Fe(IV)=O, a porphyrin-π-cation radical or a protein-based radical species. In cytochrome peroxidase, multifrequency (95-, 190-, 285 GHz) EPR was employed to characterize the magnetic parameters of the exchange coupled oxoferryl-tryptophane radical pair intermediate [(Fe(IV)=O) $Trp^{\bullet}+$] (Ivancich *et al* 2001). Furthermore, HF-EPR permitted the detection of a transient tyrosyl radical formed 60 s after the addition of 1 equiv of hydrogen peroxide to the wild-type CcP. Similarly, in the wild-type catalase-peroxidase of *Synechocystis* PCC6803, the combination of multifrequency EPR, isotopic labelling of tryptophane and tyrosine residues, and site-directed mutagenesis allowed the identification of the signal of Compound I [(Fe(IV)=O) $por^{\bullet}+$] and two radical intermediates, assigned to a tyrosine and a tryptophane (Ivancich *et al* 2003).

In analogy to the cofactor in peroxidases, in the freeze-quenched reaction of substrate free cytochrome P450cam with peroxy acids, a Fe(IV)=O porphyrin-π-cation radical intermediate was expected, which should be identical to the species in the natural reaction cycle (Schünemann *et al* 2004). However, a porphyrin-π-cation radical was not detectable but instead tyrosyl radicals were identified by multifrequency (9-, 94-, 190-, 285-) EPR spectroscopy. The combination of site-directed mutagenesis and EPR spectral simulations permitted us to assign the signals to Tyr-96 (in the wild type) and Tyr-75 (in a Y96F mutant). The observation was interpreted as an intramolecular electron transfer within 8 ms from the transiently formed Fe(IV)=O porphyrin-π-cation radical intermediate to the neighbouring tyrosines.

Another enzyme that generates a radical cofactor and amino acid radicals is DNA photolyase. In photolyases, a neutral flavin adenine dinucleotide radical, $FADH^{\bullet}$, is created in the course of cofactor photoreduction and in photorepair of UV-damaged DNA. A detailed knowledge of the electronic structure of $FADH^{\bullet}$ and its interaction with the protein environment was required to understand the details of the photoprocesses. Particularly, a knowledge of the G-tensor principal values was necessary to extract structural information of the transient radical pairs created in the course of the electron transfer reaction. The small G-tensor anisotropy of the $FADH^{\bullet}$ radical in *E. coli* CPD photolyase could be fully resolved with 360 GHz EPR (Fuchs *et al* 2002). The spectra are represented for illustration in figure 13 together with the molecular structure and the orientation of the G-tensor as determined by the experiments and by calculations.

Hyperfine splitting given by the anisotropic hyperfine coupling with the H(5) proton (i.e. the proton bound to the nitrogen(5) atom) is visible in the centre of the spectrum at g_y. The orientation of the G-tensor with respect to the molecular plane was obtained from its orientation to the hyperfine tensor axis of H(5), for which the location is known. New 94 GHz pulsed

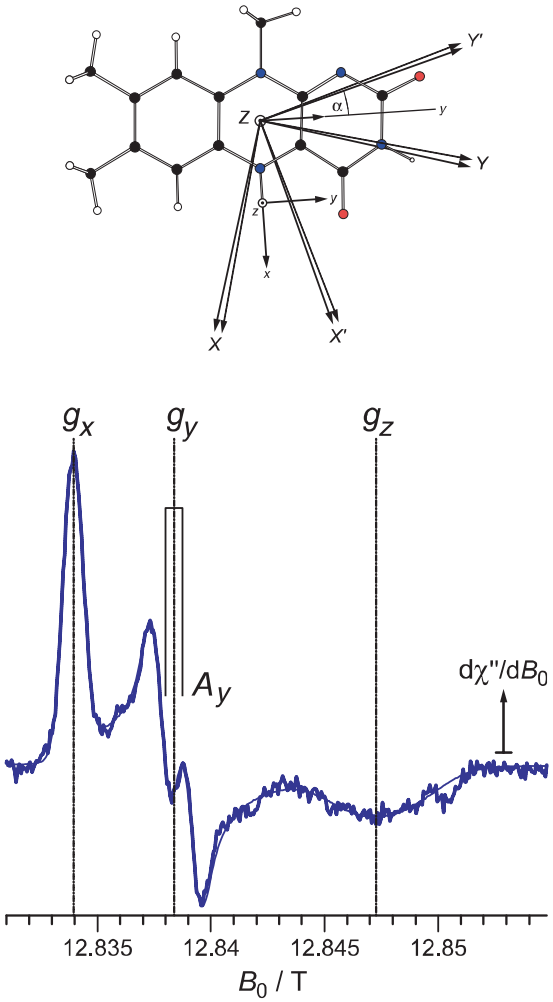

Figure 13. Experimental and simulated 360 GHz EPR spectrum of the neutral flavin radical cofactor of DNA photolyase from *E. coli*, reproduced with permission of Fuchs *et al* (2002). The molecular structure shows the G-tensor orientations X, Y, Z from experiment (straight lines) and calculations (dashed and dotted lines) and the directions of the hyperfine tensor x, y, z for the H(5) proton.

ENDOR studies are in progress to characterize the full anisotropy of the hyperfine coupling tensor of H(5) (Weber, private communication).

7.4. Metalloproteins

Metal ions and metal clusters in biological systems have been studied extensively by EPR spectroscopy since the early years (see, e.g. several reviews from the 1980s in (Hoff 1989)). $S = \frac{1}{2}$ metal complexes or clusters often exhibit substantial G-anisotropy and can be investigated conveniently at low EPR frequencies. At high frequencies, lines might become very broad and high sensitivity or high sample concentrations are required. Therefore, the advantages of HF-EPR on such systems are found predominantly with ENDOR spectroscopy, when high nuclear Zeeman resolution is desired for separation of different nuclei or in single crystal studies. For high-spin systems with ZFS, the advantages of HF-EPR have been

described in section 4. HF-EPR spectroscopy on biological systems has been carried out mostly on Mn, Cu and Fe containing proteins. To keep the discussion brief, we will not treat model complexes here but only applications on enzymes.

7.4.1. Mn-Proteins.

G-Proteins. Mn^{2+} EPR has been applied to study the metal binding site of *G*-proteins, particularly the p21ras Mn-nucleotide complex. P21ras is a small protein that plays a key role as molecular switch in the intercellular signal transduction, controlling cell growth, differentiation, apoptosis and other events (Wittinghofer and Waldmann 2000). In up to 30% of all human tumours, specific point mutations of the Ras proteins can be found. Therefore, substantial efforts have been devoted towards understanding the molecular basis for the switch function, where a GTP is bound to the protein in the ON state and a GDP in the OFF state. The nucleotide binds in the active site at a Mg^{2+} ion, which can be replaced by a paramagnetic Mn^{2+} without affecting protein activity. As the ZFS of the nucleotide-bound Mn^{2+} complex is very small ($D \sim 10$–20 mT), the ligand sphere of the ion and particularly the number of water molecules involved in the two switch states could be investigated by cw-EPR line shape analysis in solution as well as in the frozen state. At high frequencies, the $m_S = -\frac{1}{2} \rightarrow +\frac{1}{2}$ electronic transitions of this $S = \frac{5}{2}$ Mn^{2+}-complex become sufficiently narrow to permit a detailed analysis of the hyperfine couplings to ^{17}O enriched water. Initially, the analysis was performed at 140 GHz in frozen solutions of both GDP and GTP bound states (Bellew *et al* 1996, Halkides *et al* 1996). The results gave a number of coordinated water molecules in agreement with the crystal structure. However, a similar analysis performed later at room temperature for the GDP state and some representative point mutants (including an oncogenic mutant) revealed some critical differences (Rohrer *et al* 2001b) in the crystal structure. In particular, the wt-GDP species seems to exhibit one less coordinated water, i.e. probably one more coordinated amino acid, than in the crystal structure. Identification of the nature of this missing amino acid is the topic of current investigations by HF-ENDOR spectroscopy.

Concanavalin A. Concanavalin A has been recently well-studied by HF-EPR and HF-ENDOR (Goldfarb and Arieli 2004). This protein contains a Mn^{2+} centre in a slightly distorted octahedral geometry. It coordinates two water molecules, a histidine residue and three carboxylate groups. In HF-ENDOR studies on single crystals it was possible to determine the coordinates of the protons at the metal binding site that are not visible in the crystal structure (Carmieli *et al* 2001). The ^{1}H-ENDOR signals arising from the water and the histidines were assigned by comparison with spectra of crystals grown in D_2O. The rotation patterns allowed an accurate determination of the ^{1}H-hyperfine tensors and their relative orientation to the crystallographic axis. Assignment to the specific protons was done by calculating the dipolar distances within the point-dipole approximation and comparing with the x-ray structure. The results showed that both water ligands are ordered and point to the formation of H-bonds, which play a role in determining protein conformation. Comparative studies were also performed in frozen solution (Manikandan *et al* 2000). Additionally, HF-EPR spectroscopy on single crystals was used to characterize the dynamics of the binding sites. Two different Mn^{2+} sites with distinct ZFS parameters could be distinguished at low temperatures (Carmieli *et al* 2003).

Mn-superoxide dismutases. Metal specificity is an intriguing aspect of manganese and iron-containing superoxide dismutases. In spite of the high-degree of structural homology, the activity of these enzymes is highly metal-specific with complete loss of activity when the non-native metal is bound. It has been found that the HF-EPR spectra of the Mn^{2+} centres are

very sensitive to mutagenesis and inhibitor binding (Un *et al* 2001b). The 285 GHz spectra of the native enzymes from *E. coli* and *R. capsulatus* are dominated by a non-negligible zero-field interaction. Although the amino acid sequence suggests a similar trigonal bipyramidal geometry of the centre, a remarkable difference between the zero-field E parameters was established. Even more pronounced were the effects found on the spectra by complexation with azide, which converts the trigonal bipyramidal geometry into an octahedral one. The hexa-coordination strongly reduced the ZFS, giving rise to a sharp six-line spectrum. The spectra of a mutant of the cambialistic (i.e. active with both Fe and Mn) PgMnSOD protein displayed changes in the Mn^{2+} spectrum that closely resembled the spectrum of a Mn reconstituted *E. coli* Fe-SOD (Un *et al* 2004). Interestingly, this observation correlated with enzyme activity measurements that showed that this mutation, which is 11 Å away from the centre, causes loss of activity with Mn and enhanced activity with Fe, indicating a conversion from a cambialistic to an iron-specific protein.

Mn-lipoxygenase. Similarly to Mn-SODs, HF-EPR was recently employed to investigate the effect of the ligands on the ZFS of the metal centre in a new variant of lipoxygenases containing Mn (MnLO) (Gaffney *et al* 2001). Lipoxygenases are involved in the conversion of polyunsaturated fatty acids to signalling molecules in multi-step syntheses. The catalyzed reaction, peroxidation of a polyunsaturated fatty acid, involves a redox active metal centre, the fatty acid substrate, and oxygen. In these studies, the 95 and 9 GHz EPR spectra of Mn^{2+} in MnLO were analysed in detail and ZFS parameters were reported. The comparison with the ZFS values of other Mn-containing proteins such as Mn-SOD, p21ras and concanavalin A, lead to an estimate for the number of nitrogen versus oxygen ligands to the metal.

Dimanganese catalase. Catalases are redox-enzymes that catalyze the conversion of H_2O_2 into O_2 and H_2O. Most contain an iron in the active site but some reveal also two manganese ions. The catalytic cycle involves the $Mn^{2+}Mn^{2+}$ and $Mn^{3+}Mn^{3+}$ states, but a $Mn^{2+}Mn^{3+}$ and a superoxidized $Mn^{3+}Mn^{4+}$ state also exist as intermediates. Multifrequency EPR was applied to characterize the $S = \frac{1}{2}$ $Mn^{3+}Mn^{4+}$ state (Schäfer *et al* 2003). An important experimental aspect was the use of 94 GHz pulse EPR to eliminate the signals of Mn^{2+} impurities, which considerably aggravated spectral analysis. Spectral separation by T_1 and T_2 relaxation as well as by taking advantage of the different transition moments was used. The HF-EPR spectra and a multifrequency simulation strategy enabled accurate determination the G-tensor and the Mn^{55} hyperfine coupling. Comparison with spectra of $Mn^{3+}Mn^{4+}$ model complexes revealed that the magnetic properties correlate well with structural similarities such as the Mn–Mn distance, the J-coupling and the nature of the bridging ligands.

7.4.2. Copper centres. Blue copper proteins are active in redox-reaction chains in bacteria and contain a mononuclear copper centre that mediates electron transfer. The first W-band ENDOR on a metal site in protein single crystals was performed on the Cu-site in blue-copper azurin by Groenen and co-workers (Coremans *et al* 1996). The Cu ion is coordinated by five ligands, two histidines, a cysteine, a methionine and a glycine. Mims ENDOR experiments were performed at 1.2 K on the weakly coupled nitrogen nuclei, in natural abundance as well as in ^{15}N enriched samples. The spectrum recorded in the ^{15}N enriched samples is displayed in figure 14.

The contribution of five distant nitrogens could be distinguished. The full hyperfine and quadrupolar tensors could be determined for the remote nitrogens of the histidine ligands, whereas three more backbone nitrogens were identified and their hyperfine tensors were reported. The spin density was found to be delocalized over the copper ligands to parts

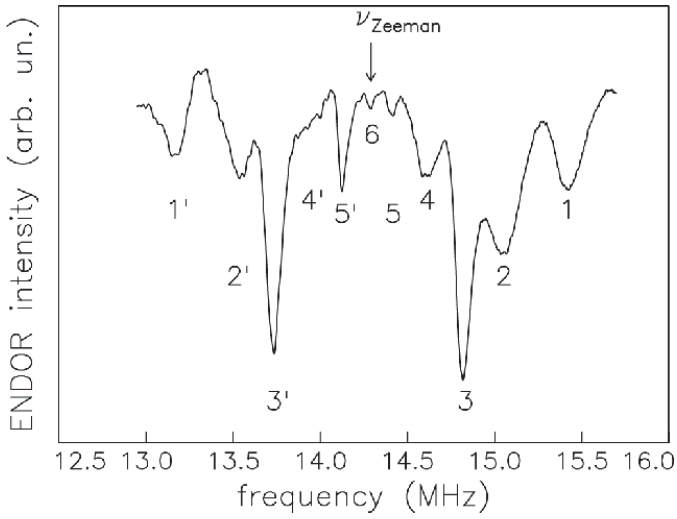

Figure 14. W-band Mims ENDOR spectrum (1.2 K) of a single crystal of fully ^{15}N-enriched azurin from *Pseudomonas aeruginosa*, reproduced with permission of Coremans *et al* (1996). The ENDOR transitions corresponding to nucleus 1 are indicated by 1 and 1′, etc. The ENDOR transition indicated by 6 coincides with the ^{15}N nuclear Zeeman frequency.

of the backbone. Further, single crystal EPR measurements were used to determine accurate g-values and the directions of the G-tensor principal axis for azurin and some mutants. The studies revealed detailed information about the orbitals involved in electron transfer (Ubbink *et al* 2002).

Another copper centre mediates electron transfer in proteins: the mixed-valence, binuclear Cu_A centre. This centre can be found, for example, in cytochrome c oxidase where it functions as the initial electron acceptor. Cu_A has a total spin $S = \frac{1}{2}$ in its oxidized form, in which each copper has a formal oxidation state of +1.5. The complex is formed by six ligands, two bridging thiolates from two cysteines, two histidines and two weak axial ligands. Recently, 95 GHz pulsed ENDOR measurements were carried out on a number of proteins containing the Cu_A centre, specifically nitrous oxide reductase, a water soluble fragment of subunit II of cytochrome c oxidase (M160T9) with its mutant (M160QT0), and the so-called purple azurin, where the Cu_A centre was engineered into azurin (Epel *et al* 2002). The ^{1}H-ENDOR spectrum consisted of two types of signals, the signals of the four strongly coupled cysteine protons and the signals of distant, weakly coupled protons. Orientation selective ENDOR and spectral simulations provided the isotropic and anisotropic parts of the hyperfine tensors. The data, along with the known copper hyperfine coupling, were employed to estimate the spin density distribution in the various centres and possible structural features were discussed. The effect of the mutation of a weak axial ligand with stronger ligands on the spin density distribution was also investigated (Slutter *et al* 2001).

Next to the Cu_A centre, cytochrome c oxidase contains a redox-inactive metal centre of unknown function. In certain organisms, this site can be occupied by a Mn^{2+} ion in the functional protein. Multifrequency (9, 35 and 95 GHz) spectroscopy has been employed to characterize this site and its interaction with the Cu_A centre (Käss *et al* 2000). As the ZFS of the Mn^{2+} centre is small, giving rise to the typical six sharp EPR lines at high frequencies, the dipolar interaction to the Cu_A could be detected. The difference in the EPR spectra between the reduced and oxidized states could be unambiguously attributed to the redox states of the Cu_A centre and the distance to the centre was determined.

7.4.3. Fe-proteins. Several HF-EPR studies have been devoted to the characterization of the Fe^{3+} ion in haemoglobin, myoglobin and their NO binding complexes. These studies have been recently summarized in review articles, to which we refer for simplicity (Hagen 1999, Andersson and Barra 2002, Hüttermann and Kappl 2002).

A large class of biological systems is represented by the FeS proteins, that contain a variety of paramagnetic clusters (Mouesca and Lamotte 1998). However, these species have been predominantly characterized at low EPR frequencies due to their characteristic large G-anisotropy. Only a few cases have been investigated by HF-EPR spectroscopy, mostly when the interaction of the $S = \frac{1}{2}$ cluster with additional paramagnetic centres was involved and HF-EPR could provide an additional means of disentangling the spectra. For instance, in trimethylamine dehydrogenase a flavin radical couples magnetically to a reduced $[4Fe–4S]^{+}$ cluster, giving rise to a triplet EPR spectrum. The use of multifrequency EPR (9–340 GHz) and numerical simulations (Fournel *et al* 1998), allowed the determination of the full set of parameters describing the magnetic interactions, in particular to establish an antiferromagnetic coupling between the two species.

In the catalytic cycle of heterodisulfide reductase from *Methanogenic Archea*, an active FeS cluster is directly involved in the chemistry of substrate reduction and has been proposed to stabilize a thiyl radical intermediate. Multifrequency (9 and 94 GHz) ^{57}Fe ENDOR was employed to identify the iron sites of this new species. The high frequency spectra recorded at 4 K were completely polarized, providing additional resolution and information as compared to the X-band data. Simulations of the orientation selected spectra and analysis of the polarization patterns revealed that this species is a substrate-bound $[4Fe4S]^{3+}$ cluster (Bennati *et al* 2004b).

In acetyl-CoA synthase, a [4Fe–4S] cluster is bridged to a binuclear CuNi or to a NiNi centre. Multifrequency EPR (3–130 GHz) was used to study the electronic structure of a new paramagnetic centre formed in the NiNi enzyme. The results supported an electronic structure where the $[4Fe–4S]^{2+}$ cluster (net $S = 0$) is bridged to Ni^{1+} ($S = \frac{1}{2}$), which is bridged to the second planar four-coordinate Ni^{2+} ($S = 0$) species (Seravalli *et al* 2004).

7.5. Nitroxide spin label studies

Nitroxide spin labels have been used for over thirty years to measure ordering and motion of phospholipid membranes by EPR spectroscopy (Berliner 1976). The nitroxide spin probes attached to the lipid chains can be used as sensitive monitors of the local polarity (Kurad *et al* 2003) and of the protein dynamics (Freed 1976). The spectra are dominated by the strongly anisotropic hyperfine coupling of the nitrogen at low magnetic field values and by the anisotropic G-tensor components at magnetic field strengths above 1 T. Both these anisotropic interactions are very sensitive to motional dynamics and to the polarity of the solvent. The motional dynamics of the nitroxide spin labels are typically rather complex superpositions of the locally restricted dynamics of the spin label itself and the slower overall dynamics of the membrane. A detailed picture of these motions can nowadays be obtained by a combination of multifrequency cw-EPR spectra, temperature dependent measurements and pulsed two-dimensional EPR experiments (Budil *et al* 1996). A knowledge of the molecular motion of the nitroxide spin label is a prerequisite for extracting other information out of the EPR spectra, such as for example the ordering of the membrane under various conditions. The theory for the analysis of these data sets, based on the stochastic Liouville equation, has been developed by Freed (Schneider and Freed 1989).

The HF-EPR spectra have a stronger orientation dependence than the low-field X-band EPR spectra and allow a more precise determination of the ordering of the membranes under the influence of cholesterol or hydration (Gaffney and Marsh 1998, Mangels *et al* 2001,

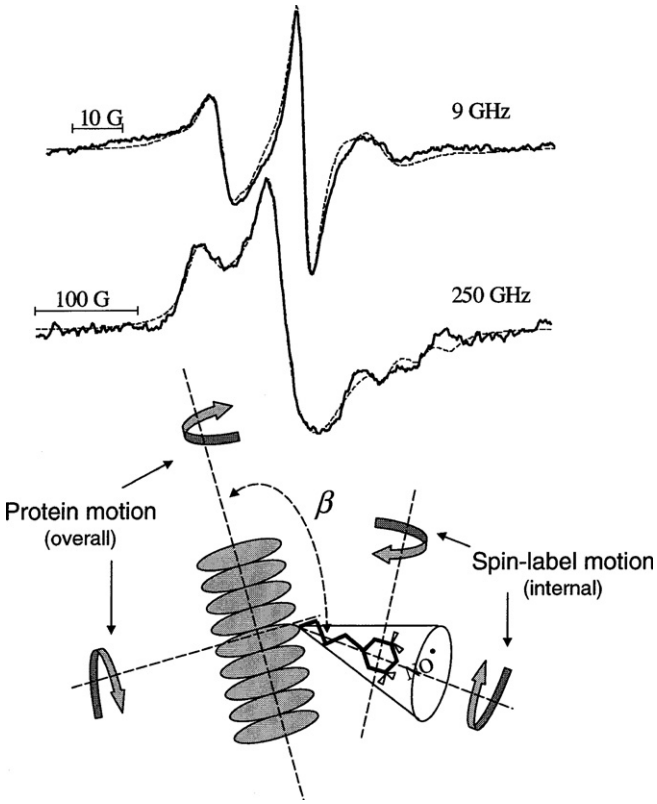

Figure 15. Multifrequency EPR study of nitroxide spin-labelled T4 lysozyme in aqueous solution, adapted with permission of Borbat *et al* (2001). The derivative spectra are for the spin label on residue 44 and are taken at 10°C. The relevant molecular motions are shown schematically in the lower part of the figure.

Ge and Freed 2003, Kurad *et al* 2004). Additionally, the cw HF-EPR spectra are less sensitive to the overall membrane and phospholipid dynamics because the dynamical sensitivity range is shifted to shorter correlation times. As the G-tensor is resolved, the anisotropy of the motion permits an accurate determination of the local dynamics of the bound spin label (Livshits and Marsh 2004) (Borbat *et al* 2001). A multifrequency EPR approach allows the investigation of the complex overall dynamics of such membranes (Liang and Freed 1999). Polarity profiles across biological membranes are essential determinants of the cellular permeability barrier and of the stability of transmembrane proteins. These profiles can be sensitively monitored by EPR spectroscopy because the A_z as well as the g_x components of the hyperfine and G-tensors of the nitroxides are very sensitive to this parameter (Kurad *et al* 2003).

The advent of site specific spin labelling in proteins by cysteine mutation launched new interest in nitroxide spin labels for the structural and dynamical characterization of proteins in the field of EPR, liquid-state as well as solid-state NMR. For EPR, all the methodology discussed above for spin-labelled lipid-chains can be directly transferred to the protein-bound spin labels (Earle and Smirnov 2004).

HF-EPR spectroscopy has been used in soluble proteins and peptides to monitor the anisotropy of the spin label dynamics at specific positions of the protein sequence (Barnes *et al* 1999, Bennati *et al* 1999b, Finiguerra *et al* 2003). An example of a multifrequency EPR study on a spin-labelled T4 lysozyme in aqueous solution is shown in figure 15 (Borbat *et al* 2001)

(Barnes *et al* 1999). The EPR spectra could be well described by a microscopic ordering with macroscopic disordering (MOMO) model and the relevant molecular motions of the spin label and the protein are shown schematically in figure 15.

Site directed spin labelling can also be used for structural studies of membrane bound proteins. The G- as well as the A-tensor of the spin label are sensitive to the polarity of the surrounding of the spin label location. Because the g_x component has an additional strong dependence on hydrogen bonding, the determination of both parameters allows polar versus non-polar as well as protic versus non-protic environments at the specific spin-labelled position to be distinguished. This, combined with the relaxation sensitivity to molecular oxygen (inner membrane) or to chromium oxalate (membrane/water interface), allows a detailed characterization of the location of the spin labelled loops of the protein, as has been demonstrated on bacteriorhodopsin (Steinhoff *et al* 2000). The same methods have been applied to investigate the conformation of a pore-forming colicin A bacterial toxin upon membrane association of the protein. A penknife-like arrangement of the helices could be favoured against an umbrella-like arrangement (Savitsky *et al* 2004).

If the protein is spin labelled at two positions, the dipolar coupling can be used to measure the distance between the two nitroxides in the protein. Short distances ($r < 2$ nm) are best accessible by cw-EPR spectroscopy (Rabenstein and Shin 1995). The method allowed, for example, an α-helical structure in a sequence part of bacteriorhodopsin to be proved (Hubbel and Altenbach 1994). At high magnetic field strengths, this interaction can be resolved orientationally dependent, providing not only the distance but also the relative orientation between the two spin labels (Hustedt *et al* 1997, Earle and Smirnov 2004). Nevertheless, the measurement of short distances is affected by the local dynamics of the spin labels and by local structural changes, which might be introduced by the insertion of the spin label in the sequence. Longer distances ($r < 8$ nm) between the two spin labels can be detected by pulsed methods (PELDOR). The current implementation of this method to HF-EPR will open new possibilities for the long range structural characterization of proteins or protein complexes.

Acknowledgments

We thank J Freed, D Goldfarb, E Groenen, F Lendzian, W Lubitz, S Un and S Weber for the permission to reproduce figures from their published work. We gratefully acknowledge our co-workers V Denisenkov, M Hertel, M Penning de Vries, M Rohrer and O Brügmann for their scientific contributions to our 180 GHz pulsed EPR, ENDOR and ELDOR spectrometer as well as B Endeward, T Maly and V Mugnaini for proof-reading our manuscript.

References

Alpert Y, Couder Y, Tuchendler J and Thome H 1973 *Biochim. Biophys. Acta* **322** 34

Andersson K K and Barra A L 2002 *Spectrochim. Acta* A **58** 1101

Bajaj V S, Farrar C T, Horstein M K, Mastovsky I, Vieregg J, Bryant J, Elena B, Kreischer K E, Temkin R J and Griffin R G 2003 *J. Magn. Reson.* **160** 85

Bar G, Bennati M, Nguyen H T, Ge J, Stubbe J and Griffin R G 2001 *J. Am. Chem. Soc.* **123** 3569

Barnes J P, Liang Z, Mchaourab H S, Freed J H and Wayne L H 1999 *Biophys. J.* **76** 3298

Becerra L R, Gerfen G J, Temkin R J, Singel D J and Griffin R G 1993 *Phys. Rev. Lett.* **71** 3561

Bellew B F, Halkides C J, Gerfen G J, Griffin R G and Singel D J 1996 *Biochemistry* **35** 12186

Bennati M, Farrar C T, Bryant J A, Inati S J, Weis V, Gerfen G J, Riggs-Gelasco P, Stubbe J and Griffin R G 1999a *J. Magn. Reson.* **138** 232

Bennati M, Fritscher J, Antonic J, Wnuk S, Bar G, Robblee J H, Kacprzak S, Kaupp M, Griffin R G and Stubbe J 2004b *7th European Biological Inorganic Chemistry Conference (Garmisch-Partenkirchen)*

Bennati M, Gerfen G J, Martinez G, Griffin R G, Singel D J and Millhauser G L 1999b *J. Magn. Reson.* **139** 281

Bennati M, Stubbe J and Griffin R G 2001 *Appl. Magn. Reson.* **21** 389
Bennati M, Weber A, Antonic J, Perlstein D L, Robblee J and Stubbe J 2003 *J. Am. Chem. Soc.* **125** 14988
Bennati M, Weiden N, Dinse K-P and Hedderich R 2004 *J. Am. Chem. Soc.* **126** 8378
Bennebroek M T and Schmidt J 1997 *J. Magn. Reson.* **128** 199
Berliner L 1976 *Spin Labeling: Theory and Applications* (New York: Academic)
Bhartia P and Bahl I J 1984 *Millimeter Wave Engineering and Applications* (New York: Wiley-Interscience)
Bittl R and Zech S G 2001 *Biochim. Biophys. Acta* **1507** 194
Bleifuss G, Kolberg M, Pötsch S, Hofbauer W, Bittl R, Lubitz W, Gräslund A, Lassmann G and Lendzian F 2001 *Biochemistry* **40** 15362
Blok H, Disselhorst J A J M, Orlinskii S B and Schmidt J 2004a *SENTINEL Meeting (Leiden)*
Blok H, Disselhorst J A J M, Orlinskii S B and Schmidt J 2004b *J. Magn. Reson.* **166** 92
Borbat P P, Costa-Filho A J, Earle K A, Moscicki J K and Freed J 2001 *Science* **291** 266
Bratt P J, Heathcote P, Hassan A K, van Tol J, Brunel L-C, Schrier J and Angerhofer A 2003 *Chem. Phys.* **294** 277
Bratt P J, Ringus E, Hassan A K, van Tol H, Maniero A L, Brunel L-C, Rohrer M, Bubenzer-Hange C, Scheer H and Angerhofer A 1999 *J. Phys. Chem.* B **103** 10973
Bratt P J, Rohrer M, Krzystek J, Evans M C W, Brunel L-C and Angerhofer A 1997 *J. Phys. Chem.* B **101** 9686
Bruker EPR Division 2000 *Bruker Rep.* **148**
Brunel L C, Barra A L and Martinez G 1995 *Physica* B **204** 298
Budil D E, Lee S, Saxena S and Freed J H 1996 *J. Magn. Reson.* A **120** 155
Burghaus O, Rohrer M, Götzinger T, Plato M and Möbius K 1992 *Meas. Sci. Technol.* **3** 765
Cardin J T, Kolaczkowski S V, Anderson J R and Budil D E 1999 *Appl. Magn. Reson.* **16** 273
Carl P, Heilig R, Maier D C, Höfer P and Schmalbein D 2004 *Bruker Rep.* **154/155** 35
Carmieli R, Manikandan P, Epel B, Kalb A J, Schnegg A, Savitsky A, Möbius K and Goldfarb D 2003 *Biochemistry* **42** 7863
Carmieli R, Manikandan P, Kalb A J and Goldfarb D 2001 *J. Am. Chem. Soc.* **123** 8378
Coremans J W A, Poluetkov O G, Groenen E J J, Canters G W, Nar H and Messerschmidt A 1996 *J. Am. Chem. Soc.* **118** 12141
Dalton L R and Kwiram A L 1972 *J. Chem. Phys.* **57** 1132
Davies E R 1974 *Phys. Lett.* A **47** 1
Deisenhofer J, Epp O, Miki K, Huber R and Michel H 1986 *Nature* **318** 618
Denisenkov V, Prisner T, Stubbe J and Bennati M 2004 *Appl. Magn. Reson.* at press
Disselhorst J A J M, van der Meer H, Poluektov O G and Schmidt J 1995 *J. Magn. Reson.* **116** 183
Dorlet P, Ling X, Sayre R T and Un S 2001 *J. Biol. Chem.* **276** 22313
Dorlet P, Rutherford A W and Un S 2000 *Biochemistry* **39** 7826
Dorlet P, Seibold S A, Babcock G T, Gerfen G J, Smith W L, Tsai A and Un S 2002 *Biochemistry* **41** 6107
Duboc-Toia C, Hassan A K, Mulliez E, Ollagnier-de Choudens S, Fontecave M, Leutwein C and Heider J 2003 *J. Am. Chem. Soc.* **125** 38
Earle K, Budil D E and Freed J H 1996 *Adv. Magn. Opt. Reson.* **19** 253
Earle K and Smirnov A I 2004 High field ESR: applications to protein structure and dynamics *Very High Frequency (VHF) ESR/EPR* vol 22, ed O Grinberg and L Berliner (New York: Plenum)
Epel B, Arieli D, Baute D and Goldfarb D 2003 *J. Magn. Reson.* **164** 78
Epel B, Pöppl A, Manikandan P, Vega S and Goldfarb D 2000 *J. Magn. Reson.* **148** 388
Epel B, Slutter C S, Neese F, Kroneck P M H, Zumft W G, Pecht I, Farver O, Lu Y and Goldfarb D 2002 *J. Am. Chem. Soc.* **124** 8152
Faller P, Rutherford A W and Un S 2000 *J. Phys. Chem.* B **104** 10960
Finiguerra M G, van Amsterdam I M C, Alagaratnam S, Ubbink M and Huber M 2003 *Chem. Phys. Lett.* **382** 528
Fournel A, Gambarelli S, Guigliarelli B, More C, Asso M, Chouteau G, Hille R and Bertrand P 1998 *J. Chem. Phys.* **109** 10905
Freed J 2000 *Annu. Rev. Phys. Chem.* **51** 655
Freed J H 1976 *Spin Labeling: Theory and Applications* ed L Berliner (New York: Academic)
Fuchs M R, Prisner T F and Möbius K 1999 *Rev. Sci. Instrum.* **70** 3681
Fuchs M R, Schleicher E, Schnegg A, Kay C W M, Törring J T, Bittl R, Bacher A, Richter G, Möbius K and Weber S 2002 *J. Phys. Chem.* B **106** 8885
Fuchs M R, Schnegg A, Plato M, Schulz C, Müh F, Lubitz W and Möbius K 2003 *Chem. Phys.* **294** 271
Fuhs M, Schnegg A, Prisner T, Köhne I, Hanley J, Rutherford A W and Möbius K 2002 *Biochim. Biophys. Acta* **1556** 81
Gaffney B J and Marsh D 1998 *Proc. Natl Acad. Sci. USA* **95** 12940
Gaffney B J, Su C and Oliw E H 2001 *Appl. Magn. Reson.* **21** 411

Ge M and Freed J 2003 *Biophys. J.* **85** 4023
Gerfen G J, Bellew B F, Griffin R G, Singel D J, Ekberg C A and Whittaker J W 1996 *J. Phys. Chem.* **100** 16739
Gerfen G J, Bellew B F, Un S, Jr J M B, Stubbe J, Griffin R G and Singel D J 1993 *J. Am. Chem. Soc.* **115** 6420
Gerfen G J, van der Donk W A, Yu G, Farrar C, Griffin R G, Stubbe J, McCarthy J R, Matthews D P and Jarvi E T 1998 *J. Am. Chem. Soc.* **120** 3823
Goldfarb D and Arieli D 2004 *Annu. Rev. Biophys. Biomol. Struct.* **33** 441
Goldfarb D, Epel B, Zimmermann H and Jeschke G 2004 *J. Magn. Reson.* **168** 75
Goldfarb D and Krymov V 2004 W-band pulsed ENDOR of transition metal centers in orientationally disordered systems and single crystals *Very High Frequency (VHF) ESR/EPR* vol 22, ed O Grinberg and L Berliner (New York: Plenum)
Goldfarb D, Strohmaier K G, Vaughan D E W, Thomann H, Poluektov O G and Schmidt J 1996 *J. Am. Chem. Soc.* **118** 4665
Grinberg O and Berliner L J 2004 *Very High Frequency (VHF) ESR/EPR* (New York: Plenum)
Grishin Y A, Fuchs M R, Schnegg A, Dubinskii A A, Dumesh B S, Rusin F S, Bratman V L and Möbius K 2004 *Rev. Sci. Instrum.* **75** 2926
Gromov I, Krymov V, Manikandan P, Arieli D and Goldfarb D 1999 *J. Magn. Reson.* **139** 8
Hagen W R 1999 *Coord. Chem. Rev.* **190–192** 209
Halkides C J, Bellew B F, Gerfen G J, Farrar C T, Carter P H, Ruo B, Evans D A, Griffin R G and Singel D J 1996 *Biochemistry* **35** 12194
Hassan A K, Maniero A L, van Tol J, Saylor C and Brunel L C 1999 *Appl. Magn. Reson.* **16** 299
Heinen U *et al* 2004 *J. Phys. Chem.* B **108** 9498
Hertel M, Bennati M, Denisenkov V and Prisner T 2004 *SENTINEL Meeting (Leiden)*
Hofbauer W and Bittl R 2000 *J. Magn. Reson.* **147** 226
Hofbauer W, Earle K, Dunnam C, Moscicki J K and Freed J 2004 *Rev. Sci. Instrum.* **75** 1194
Hofbauer W, Zouni A, Bittl R, Kern J, Orth P, Lendzian F, Fromme P, Witt H T and Lubitz W 2001 *Proc. Natl Acad. Sci. USA* **98** 6623
Höfer P, Maresch G G, Schmalbein D and Holczer K 1996 *Bruker Rep.* **142** 15
Hoff A 1979 *Phys. Rep.* **54** 75
Hoff A J 1989 *Advanced EPR* (Amsterdam: Elsevier)
Hoffman B M, Martinsen J and Venters R A 1984 *J. Magn. Reson.* **59** 110
Högbom M, Galander M, Andersson M, Kolberg M, Hofbauer W, Lassmann G, Nordlund P and Lendzian F 2003 *Proc. Natl Acad. Sci. USA* **100** 3209
Hubbel W L and Altenbach C 1994 *Curr. Opin. Struct. Biol.* **4** 566
Hustedt E J, Smirnov A I, Laub C F, Cobb C E and Beth A H 1997 *Biophys. J.* **74** 1861
Hüttermann J and Kappl R 2002 *Electron Paramagn. Reson.* **18** 304
Ivancich A, Dorlet P, Goodin D B and Un S 2001 *J. Am. Chem. Soc.* **123** 5050
Ivancich A, Jakopitsch C, Auer M, Un S and Obinger C 2003 *J. Am. Chem. Soc.* **125** 14093
Jordan A and Reichard P 1998 *Annu. Rev. Biochem.* **67** 71
Kacprzak S and Kaupp M 2004 *J. Phys. Chem.* B **108** 2464
Käss H, MacMillan F, Ludwig B and Prisner T 2000 *J. Phys. Chem.* B **104** 5362
Kaupp M 2003 *Ab initio* and density functional calculations of electronic *g*-tensor for organic radicals *EPR Spectroscopy of Free Radicals in Solids. Trends in Methods and Applications* ed A Lund and M Shiotani (Dordrecht: Kluwer)
Kaupp M, Remenyi C, Vaara J, Malkina O L and Malkin V G 2002 *J. Am. Chem. Soc.* **124** 2709
Kay C W M, Mennenga B, Görisch H and Bittl R 2004 *FEBS Lett.* **564** 69
Klette R, Törring J T, Plato M, Möbius K, Bönigk B and Lubitz W 1993 *J. Phys. Chem.* **97** 2015
Kolberg M, Bleifuss G, Pötsch S, Gräslund A, Lubitz W, Lassmann G and Lendzian F 2000 *J. Am. Chem. Soc.* **122** 9856
Kurad D, Jeschke G and Marsh D 2003 *Biophys. J.* **85** 1025
Kurad D, Jeschke G and Marsh D 2004 *Biophys. J.* **86** 264
Kutter C, Moll H P, van Toll J, Zuckermann H, Maan J C and Wyder P 1995 *Phys. Rev. Lett.* **74** 2915
Labahn A and Huber M 2001 *Appl. Magn. Reson.* **21** 325
Lakshmi K V, Poluektov O G, Reifler M J, Wagner A-M, Thurnauer M C and Brudvig G W 2003 *J. Am. Chem. Soc.* **125** 5005
Lakshmi K V, Reifler M J, Brudvig G W, Poluektov O G, Wagner A-M and Thurnauer M C 2000 *J. Am. Chem. Soc.* **104** 10445
Lawrence C C, Bennati M, Obias H V, Bar G, Griffin R G and Stubbe J 1999 *Proc. Natl Acad. Sci. USA* **96** 8979
Liang Z and Freed J H 1999 *J. Phys. Chem.* B **103** 6384

Livshits V A and Marsh D 2004 HF EPR spectra of spin labels in membranes *Very High Frequency (VHF) ESR/EPR* vol 22, ed O Grinberg and L Berliner (New York: Plenum)
Lubitz W and Feher G 1999 *Appl. Magn. Reson.* **17** 1
Lynch B, Earle K and Freed J 1988 *Rev. Sci. Instrum.* **59** 1345
MacMillan F, Hanley J, van der Weerd L, Knüpling M, Un S and Rutherford A W 1997 *Biochemistry* **36** 9297
Mangels M L, Harper A C, Smirnov A I, Howard K P and Lorigan G A 2001 *J. Magn. Reson.* **151** 253
Manikandan P, Carmieli R, Shane T, Kalb A J and Goldfarb D 2000 *J. Am. Chem. Soc.* **122** 3488
Manikandan P, Epel B and Goldfarb D 2001 *J. Am. Chem. Soc.* **40** 781
Michel H 1982 *J. Mol. Biol.* **158** 567
Millhauser G L and Freed J H 1984 *J. Chem. Phys.* **81** 37
Milov A D, Ponomarev A B and Tsvetkov Y D 1984 *Chem. Phys. Lett.* **110** 67
Mouesca J-M and Lamotte B 1998 *Coord. Chem. Rev.* **178–180** 1573
Muller F, Hopkins M A, Coron N, Grynberg M, Brunel L C and Martinez G 1989 *Rev. Sci. Instrum.* **60** 3681
Ondar M, Grinberg O Y, Dubinskii A A, Shestakov A F and Lebedev Y S 1983 *Khim. Fiz-Khim. Prir. Sint. Polim.* **86** 54
Pashenko S V, Gast P and Hoff A J 2001 *Appl. Magn. Reson.* **21** 325
Petrenko A, Maniero A L, van Tol J, MacMillan F, Li Y, Brunel L-C and Redding K 2004 *Biochemistry* **43** 1781
Poluektov O G, Utschig L M, Dubinskii A A and Thurnauer M C 2004 *J. Am. Chem. Soc.* **126** 1644
Prisner T 2004 Pulsed high-frequency EPR *Very High Frequency (VHF) ESR/EPR* vol 22, ed O Grinberg and L Berliner (New York: Plenum)
Prisner T, McDermott A E, Un S, Norris J R, Thurnauer M C and Griffin R G 1993 *Proc. Natl Acad. Sci. USA* **90** 9485
Prisner T, Rohrer M and Moebius K 1994 *Appl. Magn. Reson.* **7** 167
Prisner T, van der Est A, Bittl R, Lubitz W, Stehlik D and Möbius K 1995 *Chem. Phys.* **194** 361
Prisner T F 1997 *Adv. Magn. Opt. Reson.* **20** 245
Prisner T F, Un S and Griffin R G 1992 *Israel J. Chem.* **32** 357
Rabenstein M D and Shin Y K 1995 *Proc. Natl Acad. Sci. USA* **92** 8239
Rist G H and Hyde J S 1970 *J. Chem. Phys.* **52** 4633
Rohrer M, Brügmann O, Kinzer B and Prisner T F 2001a *Appl. Magn. Reson.* **21** 257
Rohrer M, Gast P, Möbius K and Prisner T 1996 *Chem. Phys. Lett.* **259** 523
Rohrer M, MacMillan F, Prisner T, Gardiner A T, Möbius K and Lubitz W 1998 *J. Phys. Chem.* B **102** 4648
Rohrer M, Plato M, MacMillan F, Grishin Y, Lubitz W and Möbius K 1995 *J. Magn. Reson.* A **116** 59
Rohrer M, Prisner T, Brügmann O, Käss H, Spoerner M, Wittinghofer A and Kalbitzer H R 2001b *Biochemistry* **40** 1884
Savitsky A, Kühn M, Duche D, Möbius K and Steinhoff H-J 2004 *J. Phys. Chem.* B **108** 9541
Schäfer K-O, Bittl R, Lendzian F, Barynin V, Weyhermüller T, Wieghardt K and Lubitz W 2003 *J. Phys. Chem.* B **107** 1242
Schnegg A, Fuhs M, Rohrer M, Lubitz W, Prisner T and Möbius K 2002 *J. Phys. Chem.* B **106** 9454
Schneider D J and Freed J H 1989 *Spin Labeling: Theory and Applications* vol 8, ed L Berliner (New York: Plenum) p 1
Schneider-Muntau H J, Brandt B L, Brunel L C, Cross T A, Edison A S, Marshall A G and Reyes A P 2004 *Physica* C **346** 643
Schünemann V, Lendzian F, Jung C, Contzen J, Barra A L, Sligar S G and Trautwein A X 2004 *J. Biol. Chem.* **279** 10919
Schweiger A and Jeschke G 2001 *Principles of Pulse Electron Paramagnetic Resonance* (Oxford: Oxford University Press)
Selmer T and Andrei P I 2001 *Eur. J. Biochem.* **238** 1363
Seravalli J, Xiao Y, Gu W, Cramer S P, Antholine W E, Krymov V, Gerfen G J and Ragsdale S W 2004 *Biochemistry* **43** 3944
Slutter C S, Gromov I, Epel B, Pecht I, Richards J H and Goldfarb D 2001 *J. Am. Chem. Soc.* **123** 5325
Smith G M, Le Surf J C G, Mitchell R H and Riedi P C 1998 *Rev. Sci. Instrum.* **69** 3924
Smith G M and Riedi P C 2000 *Electron Paramagn. Reson.* **17** 164
Stehlik D, Bock C H and Petersen J 1989 *J. Phys. Chem.* **93** 1612
Stehlik D and Möbius K 1997 *Annu. Rev. Phys. Chem.* **48** 739
Steinhoff H-J, Savitsky A, Wegener C, Pfeiffer M, Plato M and Möbius K 2000 *Biochim. Biophys. Acta* **1457** 253
Stubbe J and van der Donk W A 1998 *Chem. Rev.* **98** 705
Tan X, Bernardo M, Thomann H and Scholes C P 1994 *J. Chem. Phys.* **102** 2674
Teutloff C, Hofbauer W, Zech S G, Stein M, Bittl R and Lubitz W 2001 *Appl. Magn. Reson.* **21** 363
Ubbink M, Worrall J A R, Canters G W, Groenen E J J and Huber M 2002 *Annu. Rev. Biophys. Biomol. Struct.* **31** 393

Un S, Atta M, Fontecave M and Rutherford A W 1995 *J. Am. Chem. Soc.* **117** 10713
Un S, Dorlet P and Rutherford A W 2001a *Appl. Magn. Reson.* **21** 341
Un S, Dorlet P, Voyard G, Tabares L C and Cortez N 2001b *J. Am. Chem. Soc.* **123** 10123
Un S, Tabares L C, Cortez N, Hiraoka B Y and Yamakura F 2004 *J. Am. Chem. Soc.* **126** 2720
van Dam P J, Willems J, Schmidt P P, Pötsch S, Barra A L, Hagen W R, Hoffman B M, Anderson K K and Gräslund A 1998 *J. Am. Chem. Soc.* **120** 5080
van der Donk W, Stubbe J, Gerfen G J, Bellew B F and Griffin R G 1995 *J. Am. Chem. Soc.* **117** 8908
van der Est A, Prisner T, Bittl R, Fromme P, Lubitz W, Möbius K and Stehlik D 1997 *J. Phys. Chem.* B **101** 1437
Weber R T, Disselhorst J A J M, Prevo L J, Schmidt J and Wenckebach W T 1989 *J. Magn. Reson.* **81** 129
Weis V, Bennati M, Rosay M, Bryant J A and Griffin R G 1999 *J. Magn. Reson.* **140** 293
Wittinghofer A and Waldmann H 2000 *Angew. Chem. Int. Edn.* **39** 4192
Zeng R and Budil D E 2003 *Chem. Phys.* **294** 347
Zeng R, van Tol J, Deal A, Frank A and Budil D E 2003 *J. Phys. Chem.* B **107** 4624